Structural Anatomy of the Ligurian Accretionary Wedge (Monferrato, NW-Italy), and Evolution of Superposed Mélanges

[1] Andrea Festa, [2-1 & 3] Yildirim Dilek, [4-1] Giulia Codegone, [1] Simona Cavagna, and [5] Gian Andrea Pini

[1]Dipartimento di Scienze della Terra, Università degli Studi di Torino, 10125 Torino, Italy
[2]Department of Geology and Environmental Earth Science, Miami University, Oxford, OH 45056, USA
[3]State Key Laboratory of Geological Processes and Mineral Resources, School of Earth Science & Mineral Resources, China University of Geosciences, Beijing 100083, China
[4]Dipartimento di Ingegneria dell'Ambiente, del Territorio e delle Infrastrutture, Politecnico di Torino, 10129 Torino, Italy
[5]Dipartimento di Scienze Biologiche, Geologiche e Ambientali, Università di Bologna, 40127 Bologna, Italy

Corresponding Author:
Andrea Festa
Email: andrea.festa@unito.it

Re-Submitted to:
Geological Society of America Bulletin
Revised: 20 April 2013

Abstract

We document in this study the internal structure of the Late Cretaceous–late Oligocene Ligurian accretionary wedge in northwestern Italy, and the occurrence in this exhumed wedge of broken formation and three different types of mélanges that formed sequentially through time. The *Broken Formation* is the oldest unit in the accretionary wedge and shows bedding-parallel boudinage structures, which developed as a result of layer-parallel extension at the toe of the internal part of the Alpine wedge front during the Late Cretaceous–middle Eocene. This *Broken Formation* experienced an overprint of tectonic, diapiric and sedimentary processes as a result of continental collision in the late Oligocene. The NE-vergent thrusting and associated shortening produced a structurally ordered block-in-matrix fabric through mixing of both native and exotic blocks, forming the *Tectonic Mélange*. The concentration of overpressurized fluids along the thrust fault planes triggered the upward rise of shaly material, producing the *Diapiric Mélange*, which in turn provided the source material for the downslope emplacement of the youngest, late Oligocene *Sedimentary Mélange.* The Sedimentary Mélange units unconformably cover the collisional thrust faults, constraining the timing of the youngest episode of contractional deformation in the accretionary wedge. Our multi-scale structural analysis of the Ligurian accretionary wedge shows that tectonic, diapiric and sedimentary processes played a significant role in its evolution, and that the interplay between and the superposition of these different processes strongly controlled the dynamic equilibrium of the accretionary wedge in the NW Apennines–W Alps. This kind of polygenetic mélange development may be common in many modern and ancient accretionary complexes, and the processes involved in their formation are likely to be responsible for major tsunamic events in convergent margins.

Key words: accretionary wedge; polygenetic mélange; tectonic, diapiric and sedimentary processes; Northern Apennines; Tertiary Piedmont Basin.

1. Introduction

The shape and growth of the frontal wedge of the modern accretionary complexes repeatedly change to maintain the dynamic equilibrium in the wedge through alternating tectonic and sedimentary (i.e., gravitational) activities (e.g., Davis et al., 1983; Scholl et al., 1977; von Huene and Lallemand, 1990; Gutscher et al., 1998; Cliff and Vannucchi, 2004; Wang and Hu, 2006; Buiter, 2012; Gravelau et al., 2012; Haq, 2012). Highly sheared, disrupted and fragmented rock units and tectonic mélanges are the products of tectonics occurring along the basal décollements in accretionary wedges and out-of-sequence thrust-faults, and within the subduction channels (e.g., Karig and Sharman, 1975; Cloos, 1982; Moore and Byrne, 1987; Taira et al., 1992; Dileonardo et al., 2002; Collot et al., 2011). Mass-transport deposits and sedimentary mélanges result from slope instability in the trench-inner slope and in the upper parts of frontal wedges (e.g., Lallemand et al., 1990; Duperret et al., 1995; Goldfinger et al., 2000; von Huene et al., 2000; Collot et al., 2001; McAdoo et al., 2004; Sage et al., 2006; Mosher et al., 2008; Ogawa et al., 2011; Strasser et al., 2009, 2011). Shale and mud diapirism represent the upward rise of overpressured fluids migrating along the basal décollement or channeled along megasplay faults (e.g., Brown and Westebrook, 1988; Moore and Vrolijk, 1992; Kopf, 2002; Chamot-Rooke et al., 2006; Camerlenghi and Pini, 2009).

Mélanges commonly occur in ancient examples of exhumed accretionary wedges on-land, showing a complex internal block-in-matrix fabric that may vary both laterally and vertically (e.g., Maxwell, 1974; Cloos, 1984; Raymond, 1984; Cowan, 1985; Byrne and Fisher, 1990; Barnes and Korsch, 1991; Onishi and Kimura, 1995; Ogawa, 1998; Dilek et al., 1999, 2005; Pini, 1999; Dilek and Robinson, 2003; Codegone et al., 2012a, 2012b; Dilek et al., 2012;

Festa et al., 2010a; Ukar, 2012; Wakabayashi, 2012; Singlengton and Cloos, 2013). The primary internal structures of mélanges and mélange-forming processes are commonly obscured by subsequent deformational events, resulting in superposed and mixed mélanges types, such tectonic, sedimentary and diapirc mélanges. Much effort has been made to establish a set of useful criteria by which to distinguish mélange types in ancient accretionary complexes (e.g., Aalto, 1981; Naylor, 1982; Raymond, 1984; Cowan, 1985; Barber et al., 1986; Bettelli and Panini, 1989; Harris et al., 1998; Orange, 1990; Pini, 1999; Cowan and Pini, 2001; Dela Pierre et al., 2007; Yamamoto et al., 2009, 2012; Festa et al., 2010, 2012; Vannucchi and Bettelli, 2010; Festa, 2011; Osozawa et al., 2009, 2011; Wakabayashi, 2011, 2012; Codegone et al., 2012a, 2012b). These criteria are mainly based on meso-scale structural observations and analyses (e.g., Hsü, 1968; Cowan, 1985; Barber et al., 1986; Lash, 1987; Orange, 1990, Pini, 1999; Bettelli and Vannucchi, 2003) and are more rarely on map-scale or micro-scale studies (e.g., Aalto, 1981; Bettelli and Panini, 1989; Ogawa, 1998; Pini, 1999; Alonso et al., 2006; Dela Pierre et al., 2007; Festa, 2011; Saleeby, 1979, 2011; Wakabayashi, 2011, 2012; Hitz and Wakabayashi, 2012; Codegone et al., 2012a, Wakita, 2012; Vannucchi and Maltman, 2000; Kawamura et al., 2007; Michiguchi and Ogawa, 2011). However, a multi-scale approach to differentiate different chaotic rock units that were formed by different processes in accretionary wedge development has been rather limited in the literature (see, e.g., Pini, 1999; Codegone et al., 2012a, 2012b).

In this paper, we document the internal structure, tectonostratigraphic units, and geological evolution of the Ligurian accretionary wedge in Monferrato of the NW Apennines in Italy (Fig. 1) through multi-scale, field- and laboratory-based structural studies (from geological map-to meso-scale and scanning electron microscope-scale) of a composite chaotic rock unit,

previously designated as an “undifferentiated chaotic complex” (e.g., Elter et al., 1966; Bonsignore et al., 1969; Dela Pierre et al., 2003a). We differentiate the occurrence of “polygenetic mélanges” that were formed by the contemporaneous to sequential operation of tectonic, diapiric and sedimentary processes that took place to maintain the dynamic equilibrium during the evolution of this accretionary wedge. This study presents, therefore, a detailed structural anatomy of an exhumed accretionary wedge, whose evolution included both subduction-accretion and collisional tectonic events during the Late Cretaceous through late Oligocene.

2. Regional geology

The Ligurian Units in the Northern Apennines (Fig. 1) consist of the Mesozoic to early Cenozoic sedimentary successions and the Jurassic ophiolites that collectively represent the remnants of the Ligurian Ocean (Fig. 2A; see, e.g., Marroni et al., 2001; Bortolotti et al., 2005), which evolved between European plate and the Adria microplate (i.e, Africa promontory) (e.g., Coward and Dietrich, 1989; Cavazza et al., 2004, and references therein; see also Molli et al., 2010). The Internal, External and Sub-Ligurian Units (Fig. 1; e.g., Marroni et al. 2010, and references therein) contain those tectonosedimentary assemblages that were originally deposited in an oceanic basin, in an ocean-continent transition zone (OCT), and in a rifted continental margin of Adria, respectively (Fig. 2). During the Late Cretaceous through middle Eocene and prior to the continental collision, these Units were deformed and incorporated into the Alpine accretionary wedge (i.e., Principi and Treves, 1984; Marroni et al., 2001, 2010; Bortolotti et al., 2005; Vezzani et al., 2010). Here, the Ligurian Units (i.e., part of the modern Northern Apennine) and the Western Alpine Units (i.e., modern Western Alps)

were tectonically imbricated along oppositely verging (Fig. 2B), the internal (i.e. eastern) and external (i.e. western) parts of the Alpine wedge, respectively (e.g., Roure et al., 1996; Cavazza et al., 2004; Marroni et al., 2010 and reference therein).

In the middle Eocene (Figs. 2C and 2D), the east-dipping “alpine” subduction was halted due to the partial subduction of the European continental crust (e.g., Carminati et al., 2004, Marroni et al., 2010). The establishment of a West-dipping “Apennine” subduction formed an ENE-facing accretionary wedge (i.e., the proto-Apennines involving the External Ligurian Units) and involved the subduction of the thinned Adria continental margin (Figs. 2C and 2D; e.g., Marroni et al., 2010; see also Castellarin, 1994; Carminati et al., 2004; Cavazza et al., 2004; Vignaroli et al., 2008; Molli et al., 2010; Vezzani et al., 2010). As a result, the External Ligurian Units were underthrust below the Internal Ligurian Units (Figs. 2C and 2D).

Several episutural basins (Figs. 1 and 3) that developed in the proto-Northern Apennines (i.e., Epi-ligurian Units; see, e.g., Mutti et al., 1995; Ricci Lucchi, 1986) and in the internal part of the Western Alps (i.e., *Tertiary Piedmont Basin*; see Piana and Polino, 1995; Biella et al., 1997) in the middle-late Eocene cover all the accretionary wedge assemblages and related structures.

The Monferrato and Torino Hill correspond to the northern part of the late Eocene–late Miocene *Tertiary Piedmont Basin*, representing the northernmost segment of the Northern Apennines where the External Ligurian Units (i.e., the remnants of the outer part of the Ligurian accretionary wedge) crop out (e.g., Elter et al., 1966; Dela Pierre et al., 2003a; Festa et al., 2009a). Monferrato is separated from the Torino Hill by the Rio Freddo Deformation

158 Zone (*sensu* Piana and Polino, 1995) (Fig. 1). Its tectono-stratigraphic evolution occurred in
159 four main stages during the Rupelian, late Oligocene–pre late Burdigalian, late Serravallian,
160 and Messinian (see Piana, 2000; Dela Pierre et al., 2003b, 2007; Festa et al., 2005, 2009b).
161 During the Rupelian stage, NW-striking left-lateral transtensional faults associated with rifting
162 of the Balearic Sea controlled the drowning of the early Oligocene shelf along a series of NW-
163 striking pull-apart basins (Castellarin, 1994; Mutti et al., 1995). The subsequent late
164 Oligocene–pre late Burdigalian stage was marked by the northwestward migration of the
165 frontal thrust system of the Northern Apennines in Monferrato. Due to the E-W regional
166 shortening, the previously formed transtensional faults were inverted into left-lateral
167 transpressional faults, facilitating the transportation of the shelf sediments onto the slope
168 deposits. The late Burdigalian unconformity, which onlapped these transpressional faults, was
169 crosscut by the NE-SW-striking reverse faults, developed during the third tectonic stage in the
170 Serravallian. Since the late Messinian, regional N-S shortening has caused the overthrusting
171 of Monferrato and Torino Hill onto the Po Plain foredeep along the Northern Apennines frontal
172 thrust (i.e., Padane Thrust Front in Fig. 1).
173
174 **3. Chaotic rock units in Monferrato**
175
176 In Monferrato, the exhumed Ligurian accretionary wedge consists mainly of an Upper
177 Cretaceous–middle Eocene undifferentiated chaotic complex (i.e., “Undifferentiated complex”
178 *sensu* Bonsignore et al., 1969; “La Pietra chaotic complex” *sensu* Dela Pierre et al., 2003a,
179 2003b; Festa et al., 2009a, 2009b). Sacco (1935) and then Beets (1940) made the first
180 lithostratigraphic distinction in this chaotic complex on their geological maps. Elter et al.
181 (1966) and Bonsignore et al. (1969) correlated part of this undifferentiated chaotic complex

182 (i.e., the “Lauriano complex” of Albian–Cenomanian age and the “Monteu da Po Flysch” of
183 Maastrichthian age) with the “basal complex” (i.e., *Argille varicolori Auct.* and Ostia
184 sandstones) and the Monte Cassio Flysch (Cassio Unit *Auct.*) of the External Ligurian Units of
185 the Northern Apennines, respectively. However, these authors did not distinguished this
186 succession on their geological maps.
187
188 We have mapped in detail the Western Monferrato area, differentiating a lithostratigraphic
189 succession that is comparable to the upper part of the Cassio Unit of the External Ligurian
190 Units in the Northern Apennines (Figs. 3 and 4). This succession consists of the late
191 Campanian(?)–Maastrichtian Monte Cassio Flysch (Fig. 3) that overlies a composite chaotic
192 rock unit (i.e., part of the “undifferentiated complex” of Bonsignore et al., 1969). On the basis
193 of its block-in-matrix fabric, macro- and micro-structural features (observed at various scales),
194 and the nature, age and origin of its blocks (i.e., native or exotic), we have subdivided this
195 composite chaotic rock unit into a broken formation and three different types of polygenetic
196 mélanges. Each of the polygenetic mélanges represents the superposition of tectonic, diapiric
197 and sedimentary processes that reworked the block-in-matrix fabric of the broken formation
198 and the previously formed mélange/s. The broken formation corresponds to the Upper
199 Cretaceous (Santonian – Campanian) *Argille varicolori* (i.e., upper part of the “basal
200 complex”; see Figs. 3 and 4). It represents a lithostratigraphic unit resulting from the tectonic
201 dismemberment of alternating shale, sandstone and manganiferous siltstone layers.
202
203 In the following, we refer to broken formation (*sensu* Hsü, 1968) a stratally disrupted unit
204 preserving its lithological and chronological identity (see Fig. 4) and containing only “native”
205 components (i.e., intraformational origin; see also Raymond, 1984; Cowan, 1985; Pini, 1999;

206 Festa et al., 2012 and reference therein, for a complete discussion on the terms “native” and
207 “exotic”). On the contrary, we refer to “mélange” a body of mixed rocks, containing both
208 “exotic” (i.e., extraformational origin) and “native” components, in a pervasively deformed
209 matrix (see, e.g., Raymond, 1975, 1984; Silver and Beutner, 1980; Festa et al., 2012).
210 Mélanges may be formed by tectonic, sedimentary, and intrusive processes or through the
211 combination and superposition (i.e., polygenetic mélanges) of these processes (e.g.,
212 Raymond, 1984; Festa et al., 2010a and reference therein).
213
214 **3.1 Broken Formation (i.e., Upper Cretaceous *Argille varicolori*)**
215
216 The *Broken Formation* in Monferrato corresponds to the areally largest unit in the composite
217 chaotic rock unit (see *Argille varicolori* in Fig. 4). At the mesoscale, its deformation is
218 characterized by layer-parallel extension (Fig. 5A), which produced a progressive bedding-
219 parallel boudinage of cm- to m-long blocks, which are exclusively of native origin (i.e., “intra-
220 formational”). The preferred alignment and the boudinage structures of these blocks produced
221 a strong fabric, defining pseudo-bedding in the *Argille varicolori*. The more competent
222 sandstone, limestone, manganiferous siltstone, calcarenite, and marly limestone rocks show
223 a progressive stratal disruption from continuous layering to isolated, phacoidal or tabular
224 blocks in a shaly matrix. Elongated blocks (mean long-axis: 33 cm) display a high aspect ratio
225 (long axis/short axis) with a mean value ranging from 3.5 to 4 (Figs. 6A and 6B), and an
226 irregular, flat- to ellipsoidal shape corresponding to different degrees of extensional shearing
227 of the bedding plane in two orthogonal directions. Pinch-and-swell and boudinage structures
228 are mainly asymmetric, and define a planar alignment that is consistent with extensional
229 shearing in the ESE-WNW direction (Figs. 5A and 6C). R and R’ Riedel shears crosscut the

asymmetric, elongated blocks (Fig. 5A). The boudins, on the other hand, appear symmetrical in the NNE-direction (Fig. 5A).

Decimeter-wide noncylindrical, and asymmetrical intra-layer folds occur extensively throughout the *Broken Formation* (Fig. 5B). These folds are commonly rootless and transposed, and have curviplanar axial surfaces. Their fold axes display a broad girdle with two NNE-and WNW oriented maxima (Figs. 5B and 6C). The folds are sheath-like and symmetric along NNE–SSW cross-sections (Fig. 5B), whereas their limbs are asymmetrically boudinaged by R and C' shears along ESE-WNW cross-sections.

At a hand sample scale, we observe alternating layers (mm- to cm-thick) of stretched and disrupted varicolored shale, siltstone, limestone and sandstone as a result of layer-parallel extension (Figs. 5C, 5D and 5E). The more competent sandstone and limestone layers are asymmetrically boudinaged along ENE-WNW-oriented sections (Figs. 5C and 5D). The boudins are connected to each other by elongated wisps and tails, whose alignment defines a tectonically induced, pseudo-layering that is nearly parallel to the original depositional bedding (Fig. 5D). Numerous low- to high-angle normal faults and R–R' shears crosscut the more competent rocks (Fig. 5D), and continue into the weak shaly matrix as C'-type shears (*sensu* Passchier and Trouw, 2005) with only mm-scale displacements (Fig. 5E).

At the scanning electron microscope scale, the fabric of the shaly matrix is defined by the preferred alignment of the platelets of clay minerals, defining anastomosing cleavage domains with spacing of 3 to 18 μm (Fig. 5F). This fabric in the matrix is parallel to the bedding in the rocks, suggesting that sediments underwent burial-related flattening (uniaxial

layer-normal compression) during the early stages of their lithification. Disjunctive shear surfaces (C'-type shear *sensu* Passchier and Trouw, 2005, and R shear) crosscut this bedding-parallel fabric at low-angles (Fig. 5F). These structures affected both the pseudo-bedding planes and the fold limbs, indicating that intralayer folding and boudinage development on the fold limbs were spatially and temporally related (see also Vannucchi et al., 2003). Extensional-shear surfaces mimic the geometry of those observed at the hand sample scale (Figs. 5E and 5F).

3.2 Tectonic Mélange

It is characterized by a highly sheared block-in-matrix fabric (Fig. 7A) with mixed blocks of both native (e.g., limestone, sandstone and manganiferous siltstone of the *Argille varicolori*) and exotic origin. The exotic rock blocks were wrenched from the lowest stratigraphic horizons of the "basal complex" (e.g., early Cretaceous Palombini shale, Cenomanian(?)–early Campanian Scabiazza sandstone), the older buried succession (Upper Jurassic-to lower Cretaceous Maiolica limestone), the late Campanian(?)–Maastrichtian Monte Cassio Flysch, and the Upper Eocene – Oligocene *Tertiary Piedmont Basin* succession.

At the map scale (Fig. 4), the *Tectonic Mélange* defines a narrow zone (up to 50 meters wide) in the hangingwall of the NE-vergent thrust faults, emplacing the *Argille varicolori* over the Monte Cassio Flysch and the Upper Eocene–Oligocene succession of the *Tertiary Piedmont Basin*. Here, the pre-existing fabric of the *Broken Formation* is strongly overprinted and reworked by shearing associated with thrusting, forming a scale independent, "structurally ordered" block-in-matrix fabric (*sensu* Festa, 2011; see Figs. 7A and 7B). Away from the

thrust faults, the rocks gradually acquire the original, layer-parallel extensional fabric of the *Broken Formation* (Fig. 4).

At the mesoscale, the structurally ordered block-in-matrix fabric gives way to the NE-vergent (Figs. 7A and 7B) shear zones (with secondary left-lateral strike slip component of movement) caused by E-W directed regional shortening (see Figs. 6C; see also Piana, 2000; Festa et al., 2005, 2009b). The blocks in the *Tectonic Mélange* show a prevalent phacoidal shape (more rarely tabular), with mean values of their aspect ratio (long axis/short axis) ranging from 2.5 to 2.8 (Figs. 6A and 6B). Elongated blocks are imbricated in the direction of shortening and are bounded or disrupted by the anastomosing S-C shears (Figs. 7A and 7B). The exotic blocks are mixed with the native blocks derived from the *Broken Formation* along these shear zones. The long-axes of the SW-dipping native blocks (Fig. 6C) range in size from 5 cm to 90 cm with a mean length of ~20 cm (Fig. 6A). Exotic blocks are commonly larger in size (long-axis up to 125 cm, and mean length of 35 cm). The difference in size between the smaller native blocks and the larger exotic ones may be related to the nature of different processes of stratal disruption and to the thickness of the beds in the original stratigraphic succession. The mean size of the native blocks is smaller in the *Tectonic Mélange* (mean long-axis ~20 cm) than in the *Broken Formation* (mean long-axis 33 cm), indicating that the *Tectonic Mélange* developed by imposing significant tectonic strain on the earlier formed *Broken Formation.* In general, however, we observe a progressive decrease in the block size and in the intensity of tectonic mixing away from the thrust faults (Fig. 6B). This progressive decrease in the size of blocks away from the thrust faults appears to be related to the progressive decrease of mixing of native and exotic blocks.

The shaly matrix of the *Tectonic Melange* shows a pervasive NE-vergent scaly fabric (Figs. 7B and 7C) defined by anastomosing P and R shears, which are compatible with the overall reverse sense of shearing (Fig. 6C). Interlacing of disjunctive shear surfaces and the S-C fabric elements subdivides the shaly matrix into mm- to cm-long, lozenge-shaped lenses (Figs. 7B and 7C), whose surfaces are generally well polished and smooth.

Our scanning electron microscope observations also show the evidence of a pervasive S-C fabric in the shaly matrix that defines submillimetric to millimetric, sigmoidal-shaped lenses with polished and striated surfaces. These surfaces are finely spaced (few μm-to tens of μm) and envelope tabular, phacoidal (or rarely equidimensional), small clasts (5-20 μm in size) that are strongly aligned with the main fabric in the rocks (Fig. 7D). This fabric is defined by the reorientation of clay particles and elongated clasts during shear deformation.

3.3 Diapiric Mélange

Diapiric processes reworked the block-in-matrix fabric elements of both the *Broken Formation* and the *Tectonic Mélange* of the *Argille varicolori,* forming tens to hundreds of meters-wide diapiric bodies and dm- to m-wide shaly dike injections in the hanging wall units of the main thrust faults (Figs. 4 and 8A). In the field, the subvertical block-in-matrix fabric of the diapiric intrusions makes a sharp contact against the low-angle, NW-striking and “structurally ordered” fabric of the older *Broken Formation* and the *Tectonic Mélange* (Fig. 8A). In map view, the wider diapiric bodies display a roughly rounded or an elliptical shape (Figs. 4 and 8A), characterized by the concentric juxtaposition of disrupted stratigraphic horizons wrenched from both the *Argille varicolori,* the buried “basal complex”, and the older stratigraphic

succession (i.e., Scabiazza sandstone, Maiolica limestone, Palombini shale, etc.; see Fig. 8B). Irregularly shaped blocks of the Monte Cassio Flysch and some rare blocks of the Upper Eocene – Oligocene *Tertiary Piedmont Basin* succession also occur within the diapiric mélange.

At the mesoscale and in its type locality (located in the northern sector; see Fig. 8A), the diapiric bodies show internal structural zoning (*sensu* Orange, 1990; Dela Pierre et al., 2007; Festa, 2011). Their margins are characterized by a sub-vertical block-in-matrix fabric with mainly phacoidal (rarely tabular) blocks (Fig. 8B). The long axes of the blocks range from 20 cm to 40 cm, with a mean aspect ratio (long axis/short axis) of 2.5 to 2.6 (Figs. 6A and 6B). These blocks are enveloped by a varicolored shaly matrix displaying a pervasive, vertical scaly fabric (Fig. 6C) and flame-shaped injections wrapping around the blocks (Fig. 8C). The center of the diapiric bodies shows non-cylindrical folds (isoclinal-to disharmonic) with irregular axial surfaces and subvertical fold axes (Figs. 6C and 8A). The limbs of these folds have changed progressively into boudinage and pinch-and-swell features. The shaly matrix includes meter-size and larger folds traced by the sub-vertical alignment of the fragments of disrupted beds. The blocks are commonly larger in the center of the diapiric bodies than those along the margins ranging in length from 35 cm to 90 cm, and showing a mean aspect ratio (long axis/short axis) of 2.1 to 2.3 (Figs. 6A and 6B).

Scanning electron microscope observations of the shaly matrix of the diapiric bodies reveal a sub-vertical flow fabric defined by the overall alignment of the platelets of clay minerals defining anastomosing and folded cleavage domains (Fig. 8E). Surfaces of the clay platelets do not show striations. Clay particles in the center of the diapiric bodies are commonly

deformed into isoclinal or irregular and convolute folds (fold hinges 10-20 μm wide) with axial surfaces aligned parallel to the flow fabric (Fig. 8E). Cleavage domains drape around the rounded to irregularly shaped clasts. Only the long-axes of the clasts are aligned with the flow fabric (Fig. 8E). Similar convolute folds also occur near and along the margins of the diapiric bodies with less irregularly deformed and well aligned clay particles (Fig. 8F) forming sigmoidal domains that are crosscut and reoriented by the sub-vertical S-C fabric elements.

3.4 Sedimentary mélange (i.e., Polygenetic argillaceous breccias)

The *Sedimentary mélange*, here named *"Polygenetic argillaceous breccias"* (Figs. 3 and 4), has been distinguished from the *Argille varicolori*. It consists of a late Oligocene chaotic block-in-matrix unit. At the map scale (Fig. 4), the polygenetic argillaceous breccias consist of up to 50-m-thick, irregularly shaped chaotic mass-transport deposits with irregular shape that unconformably overlie both the External Ligurian Units (i.e., Monte Cassio Flysch and *Argille varicolori*) and the upper Eocene-Oligocene sedimentary rocks of the *Tertiary Piedmont Basin* (i.e., Monte Piano marls and Cardona Formation).

At the mesoscale (Fig. 9A), the block-in-matrix fabric of the argillaceous breccias is characterized by a highly disordered polymictic assemblage of rock clasts and blocks (1 cm to 15 cm in size) of different ages and origins. The clasts and blocks are mainly angular to rounded in shape (mean aspect ratio of the blocks: 1.5–1.7; Figs. 6A and 6B) and are randomly distributed in a brecciated shaly matrix. The blocks are of the same lithologies as those of the diapiric mélange, and include some material derived from the "basal complex" (i.e., *Argille varicolori*, Scabiazza sandstone, Palombini shale) and the older stratigraphic

succession (i.e., Maiolica limestone, reddish limestone) of the External Ligurian units, as well as from the Monte Cassio Flysch, and the Upper Eocene–Upper Oligocene succession of the *Tertiary Piedmont Basin* (Monte Piano marls and Cardona Formation). The shaly matrix (Fig. 9B) is typically brecciated and envelops a polymictic assemblage of sub-millimeter to cm-long, sub-angular to rounded clasts. Elongated clasts commonly display micro-faults or fractures that accommodated extensional deformation related to mass-transport movements. In the outcrop or in the hand sample, the breccias show a structureless, isotropic fabric defined by the random distribution and orientation of the clasts, dispersed in the shaly matrix (Figs. 9A, 9B and 9C).

Locally, alternating superposition of dm- to m-thick, brecciated lenticular bodies are bounded by irregular erosional surfaces and highly sheared varicolored shaly layers (Fig. 9C). This feature may have formed as a result of the repeated emplacement and superposition of minor mass-transport deposits, which demonstrate different degrees of liquefaction and variety of blocks in the shaly matrix. The extensional shearing-related features, which correspond to a narrow (up to 50 m thick) shear zone, related to the emplacement of the polygenetic argillaceous breccias, indicate direction of emplacement of the different mass-transport bodies radially away from main diapiric bodies (Fig. 10A).

In the basal part of the argillaceous breccias the fabric shows a planar anisotropy defined by the alignment of elongated blocks parallel to the extensionally sheared layers and to the erosive basal surface (Fig. 10B). This fabric is crosscut at low angles by disjunctive extensional shear surfaces (low angle Riedel shear; see Fig. 10B).

Scanning electron microscope observations show scale invariance with the mesoscopic fabric described above. The microscale fabric of the argillaceous breccias is characterized in part by rounded clasts (up to 250 μm-long) randomly distributed in a brecciated matrix, which contains strongly aligned clay particles (Fig. 9D). This matrix shows discontinuous and anastomosing surfaces wrapping around the clasts (Fig. 9E) without any trace of shearing. Only the long-axes of the clasts exhibit a common planar orientation roughly parallel to the alignment of clay particles. Spacing between the clay particles varies based on the presence or absence of clasts, and may range from ~10 to 15 μm in domains with abundant clasts, or from 3 to 5 μm where clasts are scarce or absent (Fig. 9E).

Close to the basal erosional contact, the microscale fabric of the argillaceous breccias consists of sheared extensional domains defined by the alignment of compacted clay particles (cleavage domains, 3 to 5 μm spaced) that are crosscut by low-angle, C'-type shear surfaces (*sensu* Passchier and Trouw, 2005) (Fig. 10C). Clasts here are mainly elongated and aligned parallel to the basal surface.

Decimeter- to meter-wide and up to few meter-long shale dikes intrude (Figs. 4 and 8A) the polygenetic argillaceous breccias. These dikes are composed of subvertical and convoluted injections of fluidal, red and gray shale with irregular but sharp contacts (Figs. 11A, 11B and 11C). Small, cusped and flame structures, up to dm-wide, and cm- to dm-long, commonly occur along the sharp contacts of the dikes, and intrude laterally into the country rocks (Fig. 11B and 11D). The matrix shows a sub-vertical deformational fabric wrapping around the tabular and boudinaged blocks (cm in size), which are rotated and reoriented parallel to the

421 subvertical margins of these injections (Figs. 11C and 11D). Locally, the matrix displays
422 irregular, isoclinal folds with boudinaged limbs.
423
424 The microscale fabric (SEM images) of the shale dikes shows the same characteristic,
425 vertically oriented structures commonly seen along the margins of the diapiric bodies. A
426 microscale fabric similar to that described from the core zone of the diapiric bodies occurs
427 only in the wider dike injections (few dm-wide; see Figs. 11E and 11F).
428
429 **4. Discussion**
430
431 The imprint of tectonic, sedimentary and diapiric processes is recorded at all scales (from
432 map- to micro-scale) in the fabric of the diverse chaotic rock units recognized in the "basal
433 complex" of the External Ligurian Units and in the *Tertiary Piedmont Basin* succession in
434 Monferrato (Table 1). The structural relationships between these chaotic rock units provide us
435 with an excellent opportunity to document the processes of mélange formation, their ages,
436 and the polygenetic, time-progressive tectonic evolution of the Ligurian accretionary wedge
437 during the Late Cretaceous through late Oligocene. In contrast to the Circum-Pacific
438 mélanges (e.g., the Franciscan Complex in the Western Cordillera, USA) or to those
439 metamorphic mélange units (e.g., Western Alps), in which an age-ordered stratigraphic
440 columnar section does not convey the duality in different ages of the accretionary complex
441 units (i.e., formational age versus accretionary age of the units; formational age of far-traveled
442 oceanic units versus formational age of offscraped trench sediments), the mélanges we
443 describe from Monferrato can be easily compared with other mélange occurrences all along
444 the Ligurian accretionary wedge whose stratigraphy (see Fig. 3) is readily correlated across

445 the major thrust faults. Thus, the mélanges documented in this paper provide new constraints
446 on the lateral variations (i.e., along strike) in the structural evolution of the Ligurian
447 accretionary wedge in NW Italy.
448
449 ***4.1. Late Cretaceous - middle Eocene tectonic stage***
450
451 The layer-parallel extensional block-in-matrix fabric of the *Broken Formation* (i.e., Upper
452 Cretaceous *Argille varicolori*) is consistent with a large –magnitude lateral spreading that
453 resulted in flattening (mean aspect ratio of the blocks: 3.5–4; Fig. 6B and Table 1) in two
454 orthogonal directions in unconsolidated sediments. The mechanisms responsible for this type
455 of deformation have been discussed extensively in the literature and are commonly
456 interpreted as a product of tectonic flattening across the basal shear zone of accretionary
457 wedges (e.g., Davis et al., 1983; Lash, 1987; Kimura and Mukai, 1991; Onishi and Kimura,
458 1995; Hashimoto and Kimura, 1999; Kusky and Bradley, 1999; Yamamoto, 2006) or
459 gravitational sliding on the inner trench slope (e.g., Cowan, 1985; Pini, 1999). In the Northern
460 Apennines, this deformation has been related to a shortening event which occurred in the
461 frontal and shallower levels of the Ligurian accretionary wedge (e.g., Pini, 1999; Vannucchi
462 and Bettelli, 2002; Bettelli and Vannucchi, 2003) in the latest stages of accretion, and prior to
463 the continental collision (e.g., Principi and Treves, 1984; Vai and Castellarin, 1993; Marroni
464 and Pandolfi, 1996; Pini, 1999; Bettelli and Vannucchi, 2003; Codegone et al., 2012b).
465
466 Our data and observations suggest that during the early stages of deformation, the *Argille*
467 *varicolori* underwent vertical compaction due to burial (Fig. 12), which resulted in the
468 formation of boudinage structures, in the compaction and flattening of clay particles, and the

469 decrease of porosity (Fig. 12B). When sediments made their way to the toe of the wedge,
470 compressional stress and tectonic loading produced asymmetrical boudinage and R and R'
471 shears in the more lithified layers, and C'-type shears (*sensu* Passchier and Trouw, 2005) in
472 the shaly matrix (Fig. 12C).
473
474 The coeval development of flattened, intralayer sheath–like folds, layer-parallel extensional
475 fabric, and asymmetric boudinage (Fig. 12C) might have resulted from the heterogeneity of
476 deformation at the toe of the accretionary wedge (e.g., Kimura and Mukai, 1991; Onishi and
477 Kimura, 1995; Kusky and Bradley, 1999). The undulation of the decollement surface (see
478 Onishi and Kimura, 1995) and/or the orientation of the layers with respect to σ_1 might have
479 also played a role in this heterogeneous deformation (see Kusky and Bradley, 1999). Layers
480 dipping at high angles (30°-45°) to σ_1 may have experienced both brittle extension (i.e.,
481 boudinage, R-R', C' shears and low-angle extensional faulting) and ductile contraction (i.e.,
482 folding) (Fig. 12C). Thus, at the toe of an accretionary wedge (Fig. 12A) different domains can
483 exist where layer-parallel extension develops parallel to the fold axial surfaces, and the
484 structures can be indistinguishable from the early extensional fabric related to vertical loading
485 (see Kusky and Bradley, 1999).
486
487 The above-described observations indicate that deformation started just after the deposition
488 of sediments, under unconsolidated conditions, and continued throughout progressive
489 lithification. Therefore, the age of the earliest deformation episode must have been very close
490 to the timing of deposition (i.e., Late Cretaceous-to middle Eocene). The structures related to
491 this earliest deformation stage have been sealed by the unconformable deposition of the

492 upper Eocene Monte Piano marls, which represent the base of the *Tertiary Piedmont Basin*
493 succession (Fig. 4).
494
495 ***4.2. Late Oligocene***
496
497 The layer-parallel extensional fabric of the *Broken Formation* (i.e., Upper Cretaceous *Argille*
498 *varicolori*) was overprinted and reworked by NE–vergent thrusting (with secondary left-lateral
499 strike slip component of movement) and associated shearing during the late Oligocene (Fig.
500 4). Thrusting and shearing collectively led to the development of a polygenetic mélange of a
501 tectonic origin (i.e., *Tectonic Mélange;* Figs. 13A and 13A'), characterized by a "structurally
502 ordered" block-in-matrix fabric that is consistent with the direction of inferred regional
503 shortening (see Fig. 6C). This shortening event emplaced the External Ligurian Units onto the
504 Upper Eocene–Oligocene stratigraphic units of the *Tertiary Piedmont Basin* (e.g., Piana,
505 2000; Dela Pierre et al., 2003b; Festa et al., 2005; 2009b; see also Fig. 6C), and resulted in
506 the imbrication and mixing of native and exotic blocks, mainly derived from the buried Monte
507 Cassio Flysch, the "basal complex" (i.e., Scabiazza sandstone, Palombini shale), the older
508 lithostratigraphic units (i.e., Maiolica limestone), and minor slices of the Upper Eocene–
509 Oligocene *Tertiary Piedmont Basin* succession. Exotic blocks offscraped from the footwall
510 units were accreted within the thrust shear zone and mixed with native blocks derived from
511 the earlier *Broken Formation.* The shaly varicolored matrix facilitated the concentration of
512 shearing deformation (i.e., pervasive scaly fabric and S-C shears), and together with fluid
513 focused along the fault surface helped the mobilization of hard blocks and mixing processes
514 (Figs. 13A and 13A'). The smaller size of native bocks in the *Tectonic Mélange* (mean long-
515 axis 20 cm) with respect to those in the *Broken Formation* (mean long-axis 33 cm) shows that

516 the magnitude of the tectonic strain during this thrusting event was significant. The gradual
517 transition from the *Tectonic Mélange* to the *Broken Formation*, as evidenced by decreasing of
518 both shear deformation and the occurrence of exotic blocks far from the thrust surface, shows
519 that the fault zone was not bounded by a sharp tectonic contact on top. The shaly matrix
520 accommodated thrust-related deformation along a series of several dm-thick shear zones and
521 a pervasive scaly fabric, rather than concentrating the deformation in subparallel major thrust
522 faults bounding the *Tectonic Mélange*.
523
524 The *Tectonic Mélange* differs from those ones occurring in typical subduction (e.g., Circum-
525 Pacific region) or collisional (e.g., Western Alps) settings where exotic blocks commonly
526 derived from a long-subducted footwall and/or by return flow (e.g., flow mélanges of Cloos,
527 1982). Our *Tectonic Mèlange*, that formed at shallow structural levels within the accretionary
528 wedge, provides another example in supporting that mélanges formed directly by tectonic
529 processes correspond to tectonic units structurally equivalent to mappable fault zones (see
530 Cowan, 1974; Festa et al., 2010a). For example, in fact, the block-in-matrix fabric of the San
531 Andreas fault (California) at depth, observed through drill cores, has been compared with
532 those of tectonic mélanges (see Bradbury et al., 2011).
533
534 Because of the low permeability of the *Argille varicolori*, fluids concentrated along both thrust
535 faults and micron- to mm-scale scaly cleavage surfaces reached the overpressure conditions,
536 which are required to facilitate shale diapirism (e.g., Collison, 1994; Maltman, 1994; Festa,
537 2011, Codegone et al., 2012b; see Fig. 13B). Then, overpressurized sediments exceeding the
538 hydrostatic pressure started rising upward and formed the diapiric injections. The difference in
539 the velocity gradient of the upward rising shaly material (acting as a viscous fluid), increasing

from the margins toward the core of the shale diapirs, produced an internal zoning within the diapiric bodies (Fig. 8A) (e.g., Komar, 1972; Bishop, 1978; Orange, 1990; Dela Pierre et al., 2007; Festa, 2011). This process resulted in: (i) the distribution of small phacoidal blocks (long-axis length: 20 to 40 cm; mean aspect ratio: 2.5-2.6; Figs. 6A, 6B and Table 1) along the margins of the diapiric bodies, and in their preferred alignment with the intrusive contacts; and (ii) the irregular distribution of larger, irregularly shaped blocks (long-axis length: 35 to 90 cm; mean aspect ratio: 2.1-2.3; Figs. 6A, 6B and Table 1) and the formation of irregular folds with steeply plunging axes in the cores of these diapirs. The flow fabric, as observed on the scanning electron microscope images of the samples from the cores of the diapirs (Fig. 8E), is consistent with the occurrence of overpressurized fluids without shearing. On the contrary, shearing-induced structural fabric characterizes the internal architecture of the marginal zones of the diapiric bodies (Fig. 8F).

Extrusion of the diapiric bodies on the seafloor formed topographic highs (Fig. 13B), causing the downslope mobilization of unconsolidated sediments and promoting local mass-transport movements (Fig. 13C and 13C'). These mass-transport deposits were locally augmented by the extruded diapiric material (Figs. 13C and 13C'), as evidenced by the occurrence of the same exotic and native blocks in both the diapiric and sedimentary mélanges (*Polygenetic argillaceous breccias*). Both the radial direction of extensional shearing at the base of the polygenetic argillaceous breccias and the distribution of mass-transport bodies with respect to the main diapiric bodies (Fig. 10A) are consistent with the role of diapirism in providing the source material for the emplacement of mass-transport chaotic deposits (see also Barber et al., 1986; Barber and Brown, 1988; Barber, 2013). Although, this role is well documented in modern accretionary prisms (see, e.g., Camerlenghi and Pini, 2009 and reference therein);

564 rarely has it been documented from ancient examples (see Barber, 2013 and reference
565 therein). The *Sedimentary mélanges* in Monferrato unconformably overlie and cover the thrust
566 fault, which was responsible for the emplacement of the External Ligurian Units on the upper
567 Eocene–Oligocene *Tertiary Piedmont Basin* succession. These spatial and temporal
568 relationships constrain the timing of the emplacement of the mass-transport chaotic deposits
569 as the late Oligocene (Fig. 4).
570
571 The occurrence, at all scales, of the sheared extensional fabric at the base of these mass-
572 transport chaotic deposits (Fig. 10B) and its passing upward to a random distribution of
573 rounded and irregular blocks in a brecciated matrix (Figs. 9A and 9B) is consistent with the
574 mode of debris flow and mud flow processes (e.g., Pini et al., 2012). These processes were
575 able to disaggregate, mix and reorient the fabric of the source material in the *Diapiric Mélange*
576 as also supported by the smaller size of hard blocks of the *Sedimentary Mélange* with respect
577 to that of the *Diapiric Mélange*.
578
579 The occurrence of small-scale shale dike injections piercing through the Upper Oligocene
580 *Polygenetic argillaceous breccias* suggests that the upward rise of overpressured fluids
581 locally continued during and/or after the formation of these breccias (Figs. 13C' and 13C'').
582 These shale dikes have also been documented in the Northern Apennines (Codegone et al.,
583 2012b) where, however, different causative links have been documented between tectonic,
584 sedimentary and diapiric processes, supporting that the structural and morphological
585 reconstruction of the Ligurian accretionary wedge was highly dynamic and varied along strike.
586 The combined effect of sedimentary loading provided by the early post-emplacement of the
587 *polygenetic argillaceous breccias* (i.e., dissipation of internal fluid overpressure) and the

588 discharge of fluids after the faulting stage was responsible for the emplacement of these small
589 dike injections. It is difficult to make these observations at the same scale (meters to tens of
590 meters) in mass-transport deposits in modern accretionary wedges because these types of
591 overpressured fluid features (i.e., shale dike injections) are below the standard resolution of
592 geophysical investigations. However, the documentation of a new, overpressurized fluid
593 supply following the emplacement of a *Sedimentary Mélange* may provide important
594 information on the preconditioning factors that may induce downslope remobilization of the
595 previously formed mass-transport deposits or sedimentary mélanges in modern accretionary
596 wedges. Such remobilization may trigger major tsunami events, and hence they are
597 potentially highly dangerous (see Kawamura et al., 2012).
598
599 **5. Conclusions**
600
601 The Late Cretaceous–late Oligocene Ligurian chaotic deposits exposed in Monferrato (NW
602 Italy) represent an ancient analogue of a modern convergent margin accretionary wedge. This
603 exhumed accretionary wedge includes a composite chaotic unit, known as the Upper
604 Cretaceous *Argille varicolori*, and *Tectonic*, *Diapiric* and *Sedimentary Mélanges*. The
605 youngest, *Sedimentary Mélange* is a result of the late Oligocene gravitational reworking of the
606 previously formed mélanges. All these chaotic deposits and mélanges display a record of the
607 mutual causative links among tectonic, diapiric and sedimentary processes that controlled the
608 dynamic equilibrium of the wedge through time.
609
610 A gradual transition from homogeneous to heterogeneous deformation occurred at the toe of
611 the accretionary wedge in the Late Cretaceous through middle Eocene, following the

612 deposition of the Upper Cretaceous *Argille varicolori*. The stratal disruption of this unit
613 produced the *Broken Formation* with increased shearing. The frontal part of the wedge was
614 subject to high instability during and after the continental collision in the late Oligocene. Out-
615 of-sequence thrusting (with a secondary strike-slip component of movement) in the inner
616 wedge formed the polygenetic *Tectonic Mélange*, and facilitated the mixing of exotic blocks
617 with the *Broken Formation*. The increase of fluid pressure along the thrust faults created over-
618 pressurized hydraulic conditions triggering diapiric processes, which caused the reworking of
619 the previously formed *Broken Formation* and *Tectonic Mélange*. This event developed the
620 *Diapiric Mélange*. The downslope mobilization of unconsolidated, diapiric material produced
621 the late Oligocene *Sedimentary Mélange*. These chaotic deposits of the *Sedimentary*
622 *Mélange* sealed the out-of-sequence thrust faults and marked the end of mélange formation
623 within the Ligurian accretionary wedge.
624
625 Our findings from the Late Cretaceous–late Oligocene chaotic deposits in Monferrato show
626 that the frontal wedge of an accretionary complex may evolve through a combination of
627 tectonic, diapiric and sedimentary processes that commonly overlap in time and space.
628 Studying and documenting the mode and time of these processes in both modern and ancient
629 examples of accretionary wedges is highly important and relevant in order for us to better
630 understand how the gravitational instability and tectonic processes in these convergent
631 margin products may lead to tsunamic events.
632
633
634 **Acknowledgments**

635 We thank the Science Editor Christian Koeberl for his careful editorial handling. We would like
636 to express our sincere thanks to Associate Editor Enrico Tavarnelli and Referee John
637 Wakabayashi for their constructive and thorough reviews, and useful comments from which

we have benefited greatly in revising our manuscript. We thank also F. Coscarelli, F. Dela Pierre, G. Fioraso, E. Malerba, P. Mosca and F. Piana for passionate discussions on the Ligurian Units in Monferrato.

References

Aalto, K.R., 1981, Multistage melange formation in the Franciscan Complex, northernmost California: Geology, v. 9, p. 602–607.

Alonso, J.L., Marcos, A., and Suàrez, A., 2006, Structure and organization of the Porma mélange: progressive denudation of a submarine nappe toe by gravitational collapse, American Journal of Science, v. 306, p. 32–65.

Barber, T., 2013, Mud diapirism: The origin of mélanges: cautionary tales from Indonesia: Journal of Asian Earth Sciences, early on line, http://dx.doi.org/10.1016/j.jseaes.2012.12.021.

Barber, T., and Brown, K., 1988, Mud diapirism: The origin of melanges in accretionary complexes?: Geology Today, v. 4, p. 89–94.

Barber, A.J., Tjokrosapoetro, S., and Charlton, T.R., 1986, Mud volcanoes, shale diapirs, wrench faults, and melanges in accretionary complexes, Eastern Indonesia: American Association of Petroleum Geologists Bulletin, v. 70, no. 11, p. 1729-1741.

Barnes, P.M., and Korsch, R.J., 1991, Mélange and related structures in Torlesse accretionary wedge, Wairarapa, New Zealand: New Zealand Journal of Geology and Geophysics, v. 34, p.517–532.

Beets, C., 1940, Die Geologie des Westlichen Teiles der Berge von Monferrato zwischen Turin und Murinsengo. Ein Beitrag Zur Geologie des Nortapennis: Leidsche Geologische Mededeelingen, v. 12, p. 195-250.

Bello, M., and Fantoni, R., 2002, Deep oil play in Po Valley: Deformation and hydrocarbon generation in a deformed foreland,. In: Deformation history, fluid flow reconstruction and reservoir appraisal in foreland fold and thrust belts: American Association of Petroleum Geologists, Hedberg Conference, 1–4.

Bettelli, G., and Panini, F., 1989, I mélanges dell'Appennino settentrionale tra il T. Tresinaro ed il T. Sillaro: Memorie della Società Geologica Italiana, v. 39, p. 187–214.

Bettelli, G., and Vannucchi, P., 2003, Structural style of the offscraped Ligurian oceanic sequences of the Northern Apennines: new hypotesis concerning the development of mélange block-in-matrix fabric: Journal of Structural Geology, v. 25, p. 371-388.

Biella, G., Polino, R., de Franco, R., Rossi, P.M., Clari, P., Corsi, A., and Gelati, R., 1997, The crustal structure of the Western Po Plain: reconstruction from integrated geological and seismic data: Terra Nova, v. 9, p. 28-31.

Bigi, G., Cosentino, D., Parotto, M., Sartori, R., and Scandone, P., 1983, Structural Model of Italy: Geodynamic project, C.N.R., S.El.Ca. Firenze, scale 1:500,000, 9 sheets.

689 Bishop, R.S., 1978, Mechanism for emplacement of piercement diapirs: American Association of
690 Petroleum Geologists Bulletin, v. 62, p. 1561–1583.
691
692 Bonsignore, G., Bortolami, G., Elter, G., Montrasio, A., Petrucci, F., Ragni, U., Sacchi, R., Sturani, C.,
693 and Zanella, E., 1969, Note Illustrative dei Fogli 56-57, Torino-Vercelli della Carta Geologica
694 d'Italia alla scala 1:100,000: Servizio Geologico d'Italia, Roma, 96 p.
695
696 Bortolotti, V., Marroni, M., Pandolfi, L., and Principi, G., 2005, Mesozoic to Tertiary tectonic history of
697 the Mirdita ophiolites, northern Albania: Island Arc, v. 14, p. 471-493.
698
699 Bradbury, K.M., Evans, J.P., Chester, J.S., Chester, F.M., and Kirschner, D.L., 2012, Lithology and
700 internal structure of the San Andreas fault at depth based on characterization of Phase 3 whole-
701 rock core in the San Andreas Fault Observatory at Depth (SAFOD) borehole: Earth and
702 Planetary Science Letters, v. 310, p. 131–144.
703
704 Brown, K.M., 1990, The nature and hydrogeologic significance of mud diapirs and diatremes for
705 accretionary systems: Journal of Geophysical Research, v. 95, p. 8969–8982.
706
707 Brown, K.M., and Westbrook, G.K., 1988, Mud diapirism and subcretion in the Barbados ridge
708 accretionary complex: The role of fluids in the accretionary processes: Tectonics, v. 7, p. 613–
709 640.
710
711 Buiter, S.J.H, 2012, A review of brittle compressional wedge models: Tectonophysics, v. 530-531, p.
712 1-17.
713
714 Byrne, T., and Fisher, D., 1990, Evidence for a weak overpressured décollement beneath sediment-
715 dominated accretionary prisms: Journal of Geophysical Research, v. 95, B6, p. 9081-9097.
716
717 Camerlenghi, A., and Pini, G.A., 2009, Mud volcanoes, olistostromes and Argille scagliose in the
718 Mediterranean region: Sedimentology, v. 56, p. 319-365.
719
720 Carminati, E., Doglioni, C., and Scrocca, D., 2004, Alps vs Apennine, *in* Crescenti, U., D'offizi, S.,
721 Merlino, S., and Sacchi, L., eds., Geology of Italy: Special volume of the Italian Geological
722 Society for the IGC 32 Florence-2004, p. 141–152.
723
724 Castellarin, A., 1994, Strutturazione eo-mesoalpina dell'Appennino Settentrionale attorno al "nodo
725 ligure", *in* Capozzi, R., and Castellarin, A., eds., Studi preliminari all'acquisizione dati del profilo
726 CROP 1–1A La Spezia–Alpi orientali: Studi Geologici Camerti, Volume Speciale 1992/2,
727 Camerino, Università degli Studi di Camerino, p. 99-108.
728
729 Cavazza, W., Roure, F., and Ziegler, P.A., 2004, The Mediterranean area and the surrounding
730 regions: active processes, remnants of former Tethyan oceans and related thrust belts, *in*
731 Cavazza, W., Roure, F., Spakman, W., Stampfli, G.M., and Ziegler, P.A., eds., The TRANSMED
732 Atlas: The Mediterranean Region from crust to mantle: Springer, p. 1–29.
733
734 Chamot-Rooke, N., Rabaute, A., and Kreemer, C., 2006, Western Mediterranean Ridge mud belt
735 correlates with active shear strain at the prism-backstop geological contact: Geology, 33, p. 861–
736 864.
737
738 Clift, P., and Vannucchi, P., 2004, Controls on tectonic accretion versus erosion in subduction zones:
739 Implications for the origin and recycling of the continental crust: Reviews of Geophysics, v. 42,
740 RG2001, doi:10.1029/2003RG000127.

741
742 Cloos, M., 1982, Flow melanges: Numerical modeling and geologic constraints on their origin in the
743 Franciscan subduction complex, California: Geological Society of America Bulletin, v. 93, p. 330–
744 345.
745
746 Cloos, M., 1984, Flow mélanges and structural evolution of accretionary wedges, *in* Raymond L.A.,
747 ed., Mélanges: their nature, origin and significance: Geological Society of America Special Paper
748 198, p. 71-79.
749
750 Codegone, G., Festa, A., and Dilek, Y., 2012a, Formation of Taconic mélanges and Broken formations
751 in the Hamburg Klippe, Central Appalachian orogenic belt, Eastern Pennsylvania:
752 Tectonophysics, v. 568-569, p. 215-229. doi:10.1016/j.tecto.2012.03.017
753
754 Codegone, G., Festa, A., Dilek, Y., and Pini, G.A., 2012b, Small-scale Polygenetic mélanges in the
755 Ligurian accretionary complex, Northern Apennines, Italy, and the role of shale diapirism in
756 superposed mélange evolution in orogenic belts: Tectonophysics, v. 568-569, p. 170-184.
757 doi:10.1016/j.tecto.2012.02.003
758
759 Collison, J., 1994, Sedimentary deformational structures, *in* Maltman, A., ed., The geological
760 deformation of sediments: Chapman & Hall, London, p. 96–125.
761
762 Collot, J-Y., Lewis, K., Lamrche, G., and Lallemand, S. 2001, The giant Ruatoria debris avalanche on
763 the northern Hikurangi margin, New Zealand: Result of oblique seamount subduction: Journal of
764 Geophysical Research, v. 106, B9, p. 19271-19297.
765
766 Collot, J.-Y., Ribodetti, A., Agudelo, W., and Sage, F., 2011, The South Ecuador subduction channel:
767 Evidence for a dynamic mega-shear zone from 2D fine-scale seismic reflection imaging and
768 implications for material transfer: Journal of Geophysical Research, v. 116, B11102,
769 doi:10.1029/2011JB008429.
770
771 Cowan, D.S., 1974, Deformation and metamorphism of the Franciscan Subduction Zone Complex
772 northwest of Pacheco Pass, California. Geological Society of America Bulletin: v. 85, p. 1623–
773 1634.
774
775 Cowan, D.S., 1985, Structural styles in Mesozoic and Cenozoic mélanges in the western Cordillera of
776 North America: Geological Society of America Bulletin, v. 96, p. 451-462.
777
778 Cowan, D.S., and Pini, G.A., 2001, Disrupted and chaotic rock units in the Apennines, *in* Vai, G.B.,
779 and Martini, I.P., eds., Anatomy of a Mountain Belt: The Apennines and Adjacent Mediterranean
780 Basins: Kluwer Academic Publishers, Dordrecht, p. 165-176.
781
782 Coward, M.P., and Dietrich, D., 1989, Alpine tectonics - an overview, *in* Coward, M.P., Dietrich, D.,
783 and Park, R.G., eds., Alpine tectonics: Geological Society London Special Pubblications 45, p.
784 1–29.
785
786 Davis, D., Suppe, J., and Dahlen, F.A., 1983, Mechanics of fold-and-thrust belts and accretionary
787 wedges: Journal of Geophysical Research, v. 88, p. 1153-1172.
788
789 Dela Pierre, F., Festa, A., and Irace, A., 2007, Interaction of tectonic, sedimentary and diapiric
790 processes in the origin of chaotic sediments: an example from the Messinian of the Torino Hill
791 (Tertiary Piedmont Basin, NW Italy): Geological Society of America Bulletin, v. 119, 1107-1119.
792

793 Dela Pierre, F., Piana, F., Boano, P., Fioraso, G., and Forno, M.G., 2003a, Carta Geologica d'Italia
794 alla scala 1:50,000 – Foglio 157 "Trino": ISPRA, Istituto Superiore per la Protezione e Ricerca
795 Ambientale. Ed. Litografia Geda, Nichelino, 1 Sheet.
796
797 Dela Pierre, F., Piana, F., Fioraso, G., Boano, P., Bicchi, E., Forno, M.G., Violanti, D., Clari, P., and
798 Polino, R., 2003b, Note Illustrative della Carta Geologica d'Italia alla scala 1:50,000. Figlio 157
799 "Trino": APAT, Dipartimento Difesa del Suolo, 147 p.
800
801 Dilek, Y., Thy, P., Hacker, B., and Grundvig, S., 1999, Structure and petrology of Tauride ophiolites
802 and mafic dike intrusions (Turkey): implications for the Neotethyan ocean: Geological Society of
803 America Bulletin, v. 111, p. 1192–1216.
804
805 Dilek, Y, and Robinson, P.T., 2003. Ophiolites in Earth history: Introduction, *in* Dilek, Y. and Robinson,
806 P.T. (Eds.), Ophiolites in Earth History: Geological Society of London Special Publications, vol.
807 218, p. 1-8.
808
809 Dilek, Y., Shallo, M., and Furnes, H., 2005. Rift-drift, seafloor spreading, and subduction zone
810 tectonics of Albanian ophiolites: International Geology Review, v. 47, p. 147–176.
811
812 Dilek, Y., Festa, A., Ogawa, Y., and Pini, G.A., 2012, Chaos and geodynamics: Mélanges, Mélange-
813 forming processes and their significance in the geological record: Tectonophysics, v. 568-569, p.
814 1-6.
815
816 Dileonardo, C.G., Moore, J.C., Nissen, S., and Bangs, N., 2002, Control of internal structure and fluid-
817 migration pathways within the Barbados Ridge décollement zone by strike-slip faulting: Evidence
818 from coherence and three-dimensional seismic amplitude imaging: Geological Society of
819 America Bulletin, v. 114, p. 51–63.
820
821 Duperret, A., Bourgois, J., Lagabrielle, Y., and Suess, E., 1995, Slope instabilities at an active
822 continental margin: Large-scale polyphase submarine slides along the northern Peruvian
823 margin, between 5°S and 6°S: Marine Geology, v. 122, p. 303–328, doi:10.1016/0025-
824 3227(94)00125-5.
825
826 Elter, G., Elter, P., Sturani, C., and Weidmann, M., 1966, Sur la prolongation du domaine ligure de
827 l'Apennin dans le Monferrat et les Alpes et sur l'origine de la Nappe de la Simme s.l. des
828 Préalpes romandes et chablaisannes: Archives des Sciences de Genève, v. 19, p. 279-377.
829
830 Festa, A., 2011, Tectonic, sedimentary, and diapiric formation of the Messinian mélange: Tertiary
831 Piedmont Basin (northwestern Italy), *in* Wakabayashi, J., and Dilek, Y., eds., Melanges:
832 Processes of formation and societal significance: Geological Society of America Special Paper
833 480, p. 215-232. doi: 10.1130/2011.2480(10).
834
835 Festa, A., Boano, P., Irace, A., Lucchesi, S., Forno, M.G., Dela Pierre, F., Fioraso, G., and Piana, F.,
836 2009a, Carta Geologica d'Italia alla scala 1:50,000. Foglio 156 "Torino Est". ISPRA, Istituto
837 Superiore per la Protezione e Ricerca Ambientale. Ed. Litografia Geda, Nichelino, 1 Sheet.
838
839 Festa, A., Dela Pierre, F., Irace A., Piana F., Fioraso G., Lucchesi S., Boano P., and Forno M.G.,
840 2009b, Note Illustrative della Carta Geologica d'Italia alla scala 1:50,000. Foglio 156 "Torino
841 Est": ISPRA, Istituto Superiore per la Protezione e la Ricerca Ambientale, Litografia Geda,
842 Nichelino, p. 143.
843

844 Festa, A., Dilek, Y., Pini, G.A., Codegone, G., and Ogata, K., 2012, Mechanisms and processes of
845 stratal disruption and mixing in the development of mélanges and broken formations: Redefining
846 and classifying mélanges: Tectonophysics, v. 568-569, p. 7-24. doi:10.1016/j.tecto.2012.05.021
847
848 Festa, A., Piana, F., Dela Pierre, F., Malusà, M.G., Mosca, P., and Polino, R., 2005, Oligocene-
849 Neogene kinematic constraints in the retroforeland basin of the Northwestern Alps: Rendiconti
850 della Società Geologica Italiana (nuova serie), v. 1, p. 107-108.
851
852 Festa, A., Pini, G.A., Dilek, Y., and Codegone, G., 2010a, Mélanges and mélange-forming processes:
853 a historical overview and new concepts: *in* Dilek, Y., ed., Alpine Concept in Geology:
854 International Geology Review, v. 52, nos. 10-12, p. 1040-1105. doi:
855 10.1080/00206810903557704.
856
857 Festa, A., Pini, G.A., Dilek, Y., Codegone, G., Vezzani, L., Ghisetti, F., Lucente, C.C., and Ogata, K.,
858 2010b, Peri-Adriatic mélanges and their evolution in the Tethyan realm, *in* Dilek, Y., ed.,
859 Eastern Mediterranean geodynamics (Part II): International Geology Review, v. 52, nos. 4-6),
860 p. 369-406. doi: 10.1080/00206810902949886.
861
862 Goldfinger, C., Kulm, L.D., McNeill, L.C., and Watts, P., 2000, Super-scale failure of the southern
863 Oregon Cascadia margin: Pure and Applied Geophysics, v. 157, p. 1189–1226, doi:
864 10.1007/s000240050023.
865
866 Gravelau, F., Malavieille, J., and Dominguez, S., 2012, Experimental modeling of orogenic wedges: a
867 review: Tectonophysics, v. 538-540, p. 1-66.
868
869 Gutscher, M.A., Kukowski, N., Malavieille, J., and Lallemand, S., 1998, Episodic imbricate thrusting
870 and underthrusting: Analog experiments and mechanical analysis applied to the Alaskan
871 accretionary wedge: Journal of Geophysical Research, v. 103, B5, 10, p.161–10,176,
872 doi:10.1029/97JB03541.
873
874 Haq, S.S.B., 2012, Out-of-sequence thrusting in experimental Coulomb wedges: implications for the
875 structural development of mega-spaly and forearc basins: Geophysical Research Letters, v. 39,
876 L20306, doi: 10.1029/2012GL053176
877
878 Harris, R.A., Sawyer, R.K., and Audley-Charles, M.G., 1998, Collisional melange development:
879 geologic associations of active melange-forming processes with exhumed melange facies in the
880 western Banda orogen, Indonesia: Tectonics, v. 17, n. 3, p. 458-479.
881
882 Hashimoto, Y., and Kimura, G., 1999, Underplating process from mélange formation to duplexing:
883 Example from the Cretaceous Shimanto Belt, Kii Peninsula, southwest Japan: Tectonics, v. 18,
884 p. 92–107.
885
886 Hitz, B., and Wakabayashi, J., 2012, Unmetamorphosed sedimentary mélange with high-pressure
887 metamorphic blocks in a nascent forearc basin setting: Tectonophysics, v. 568-569, p. 124-134.
888
889 Hsü, K.J., 1968, Principles of mélanges and their bearing on the Franciscan-Knoxville Paradox:
890 Geological Society of America Bulletin, v. 79, p. 1063–1074.
891
892 Karig, D.E., and Sharman, G., 1975, Accretion and subduction in Pacific trenches: Geological Society
893 of America Bulletin, v. 86, p. 377-389.
894

895 Kawamura, K., Ogawa, Y., Oyagi, N., Kitahara, T., and Anma, R., 2007, Structural and fabric analyses
896 of basal slip zone of the Jin'nosuke-dani landslide, northern central Japan: its application to the
897 slip mechanism of decollement: Landslides, v. 4, p. 371-380.
898
899 Kawamura, K., Sasaki, T., Kanamatsu, Y., Sakaguchi, A., Ogawa, Y., 2012, Large submarine
900 landslides in the Japan Trench: A new scenario for additional tsunami generation: Geophysical
901 Research Letters, v. 39, doi: 10.1029/2011GL050661.
902
903 Kimura, G., and Mukai, A., 1991, Underplated units in an accretionary complex: melange of the
904 Shimanto belt of eastern Shikoku, southwest Japan: Tectonics, v. 10, n. 1, p. 31-50.
905
906 Komar, P.D., 1972, Flow differentiation in igneous dikes and sills: Profiles of velocity and phenocryst
907 concentration: Geological Society of America Bulletin, v. 83, p. 3443–3448.
908
909 Kopf, A., 2002, Significance of mud volcanism: Reviews of Geophysics, v. 40, p. 1–51.
910
911 Kusky, T.M., and Bradley, D.C., 1999, Kinematic analysis of melange fabrics: examples and
912 applications from the McHugh Complex, Kenai Peninsula, Alaska: Journal of Structural Geology,
913 v. 21, p. 1773-1796.
914
915 Lallemand, S., Collot, J.Y., Pelletier, B., Rangin, C., and Cadet, J.P., 1990, Impact of oceanic
916 asperities on the tectonogenesis of modern convergent margins: Oceanologica Acta, v. 10, p.
917 17–30.
918
919 Lash, G.G., 1987, Diverse melanges of an ancient subduction complex: Geology, v. 15, p. 652-655.
920
921 Maltman, A., 1994, Introduction and overview, *in* Maltman, A., ed.: The geological deformation of
922 sediments. Chapman & Hall, London, p. 1–35.
923
924 Marroni, M., and Pandolfi , L., 1996, The deformation history of an accreted ophiolite sequence: The
925 internal Liguride units (northern Apennines, Italy): Geodinamica Acta, v. 9, p. 13–29.
926
927 Marroni, M., and Pandolfi, L., 2007, The architecture of an incipient oceanic basin: a tentative
928 reconstruction of the Jurassic Liguria-Piemonte basin along the Northern Apennines–Alpine
929 Corsica transect: International Journal of Earth Sciences, v. 96, p. 1059–1078.
930
931 Marroni, M., Meneghini, F., and Pandolfi, L., 2010, Anatomy of the Ligure-Piemontese subduction
932 system: evidence from Late Cretaceous–middle Eocene convergent margin deposits in the
933 Northern Apennines, Italy: International Geology Review, v. 52, p. 1160-1192.
934
935 Marroni, M., Molli, G., Ottria, G., and Pandolfi, L., 2001, Tectono-sedimentary evolution of the External
936 Liguride units (Northern Apennines, Italy): insight in the pre-collisional history of a fossil ocean-
937 continet transition zone: Geodinamica Acta, v. 14, p. 307-320.
938
939 Maxwell, J.C., 1974, Anatomy of an orogeny: Geological Society of America Bulletin, v. 85, p. 1195–
940 1204.
941
942 McAdoo, B.G., Capone, M.K., and Minder, K., 2004, Seafloor geomorphology of convergent margins:
943 Implications for Cascadia seismic hazard: Tectonics, v. 23, TC6008,
944 doi:10.1029/2003TC001570.
945

946 Michiguchi, Y., and Ogawa, Y., 2011, Implication of dark bands in Miocene–Pliocene accretionary
947 prism, Boso Peninsula, central Japan, *in* Wakabayashi, J., and Dilek, Y., eds., Melanges:
948 Processes of formation and societal significance: Geological Society of America Special Papers
949 480, p. 247-260.
950
951 Moore, J.C., and Byrne, T., 1987, Thickening of fault zones: A mechanism of melange formation in
952 accreting sediments: Geology, v. 15, p. 1040–1043.
953
954 Moore, J.C., and Vrolijk, P., 1992, Fluids in accretionary prisms: Reviews of Geophysics, v. 30, no. 2),
955 p. 113-135.
956
957 Molli, G., Crisipini, L., Malusà, G.M., Mosca, P., Piana, F., and Federico, L., 2010, Geology of the
958 Western Alps – Northern Apennines junction area: a regional review: Journal of Virtual Explorer,
959 v. 36, no. 10, doi: 10.3809/jvirtex.2010.00215
960
961 Mosca, P., Polino, R., Rogledi, S., and Rossi, M., 2010, New data for the kinematic interpretation of
962 the Alps-Apennines junction (Northwestern Italy): International Journal of Earth Science, v. 99,
963 no. 4, p. 833-849.
964
965 Mosher, D.C., Austin, J.A., Jr., Fisher, D., and Gulick, S.P., 2008, Deformation of the northern
966 Sumatra accretionary prism from high-resolution seismic reflection profiles and ROV
967 observations: Marine Geology, v. 252, p. 89–99, doi:10.1016/j.margeo.2008.03.014.
968
969 Mutti, E., Papani, L., di Biase, D., Davoli, G., Mora, S., Degadelli, S., and Tinterri, R., 1995, Il bacino
970 terziario epimesoalpino e le sue implicazioni sui rapporti tra Alpi e Appennino: Memorie della
971 Società Geologica, v. 47, p. 217–244.
972
973 Naylor, M.A., 1982, The Casanova Complex of the Northern Apennines: A mélange formed on a distal
974 passive continental margin: Journal of Structural Geology, v. 4, p. 1–18.
975
976 Ogawa, Y., 1998, Tectonostratigraphy of the Glen App area, Southern Uplands, Scotland: anatomy of
977 Ordovician accretionary complex: Journal of the Geological Society of London, v. 155, p. 651-
978 662.
979
980 Ogawa, Y., Anma, R., and Dilek, Y., 2011, Accretionary prism and convergent margin tectonics in the
981 Northwest Pacific Basin. Book Series in Modern Approaches in Solid Earth Sciences, Springer
982 Science+Business Media B.V. 2011Springer Science, Dordrecht, The Netherlands. ISBN 978-
983 90-481-884-0.
984
985 Onishi, C.T., and Kimura, G., 1995, Change in fabric of mélange in the Shimanto Belt, Japan: Change
986 in relative convergence?: Tectonics, v. 14, p. 1273–1289.
987
988 Orange, D.L., 1990, Criteria helpful in recognizing shear-zone and diapiric mélanges: examples from
989 the Hoh acretionary complex, Olympic Peninsula, Washington: Geological Society of America
990 Bulletin, v. 102, p. 935-951.
991
992 Osozawa S., Morimoto J., and Flower F.J., 2009, “Block-in-matrix” fabrics that lack shearing but
993 possess composite cleavage planes: A sedimentary mélange origin for the Yuwan accretionary
994 complex in the Ryukyu island arc, Japan: Geological Society of America Bulletin, v. 121, p.
995 1190–1203.
996

997 Osozawa S., Pavlis T., and Flowers M.F.J., 2011, Sedimentary block-in-matrix fabric affected by
998 tectonic shear, Miocene Nabae complex, Japan, *in* Wakabayashi, J., and Dilek, Y., eds.,
999 Mélanges: Processes of Formation and Societal Significance: Geological Society of America
1000 Special Paper 480, p. 189-206. doi: 10.1130/2011.2480(08)
1001
1002 Passchier, C.W., and Trouw, R.A., 2005, Microtectonics: Springer, Berlin - Heidelberg - New York, 365
1003 p.
1004
1005 Piana, F., 2000., Structural features of Western Monferrato (Alps-Apennines junction zone, NW Italy):
1006 Tectonics, v. 19, p. 943-960.
1007
1008 Piana, F., and Polino, R., 1995, Tertiary structural relationships between Alps and Apennines: The
1009 critical Torino Hill and Monferrato area: Northwestern Italy: Terra Nova, v. 7, p. 138–143.
1010
1011 Pini, G.A., 1999, Tectonosomes and olistostromes in the Argille Scagliose of the Northern Apennines,
1012 Italy: Geological Society of America Special Paper 335, 73 p.
1013
1014 Pini, G.A., Ogata, K., Camerlenghi, A., Festa, A., Lucente, C.C., and Codegone, G., 2012,
1015 Sedimentary mélanges and fossil mass-transport complexes: a key for better understanding
1016 submarine mass movements?, *in* Yamada, Y., et al., eds., Submarine mass movements and
1017 their consequences: Advances in natural and technological hazards research, 31: Springer
1018 Science+Business Media B.V., p. 585–594.
1019
1020 Principi, G., and Treves, B., 1984, Il sistema Corso-Appenninico come prisma di accrezione. Riflessi
1021 sul problema generale del limite Alpi-Appennini: Memorie della Società Geologica Italiana, v. 28,
1022 p. 549-576.
1023
1024 Raymond, L.A., 1975, Tectonite and mélange - a distinction: Geology, v. 3, p. 7–9.
1025
1026 Raymond, L.A., 1984, Classification of mélanges, *in* Raymond L.A., ed., Mélanges: their nature, origin
1027 and significance: Geological Society of America Special Paper 198, p. 7-20.
1028
1029 Remitti, F., Vannucchi, P., Bettelli, G., Fantoni, L., Panini, F., and Vescovi, P., 2011, Tectonic and
1030 sedimentary evolution of the frontal part of an ancient subduction complex at the transition from
1031 accretion to erosion: the case of the Ligurian wedge of the northern Apennines, Italy: Geological
1032 Society of America Bulletin, v. 123, n. 1-2, p. 51-70.
1033
1034 Ricci Lucchi, F., 1986, The Oligocene to recent foreland basin of the Northern Appennines, *in* Allen,
1035 P.A., and Homewood, P., eds., Foreland basins: International Association of Sedimentologists,
1036 Special Publication, v. 8, p. 105–139.
1037
1038 Roure, F., Bergerat, F., Damotte, B., Mugnier, J.L., and Polino, R., 1996, The Ecors-Crop Alpine
1039 seismic traverse: Bulletin de la Societé Géologique de France, v. 170, p. 1–113.
1040
1041 Sacco, F., 1935, Note Illustrative della Carta Geologica d'Italia alla scala 1:100,000. Fogli di Torino,
1042 Vercelli, Mortara, Carmagnola, Asti, Alessandria, Cuneo, Ceva, Genova N. e Voghera O.
1043 costituenti il bacino terziario del Piemonte. Ministero delle Corporazioni, Regio Ufficio Geologico
1044 di Roma, 85 p.
1045
1046 Sage, F., Collot, J.-Y., and Ranero, C.R., 2006, Interplate patchiness and subduction-erosion
1047 mechanisms: evidence from depth-migrated seismic images at the central Ecuador convergent
1048 margin: Geology, v. 34, n. 12, p. 997-1000.

Saleeby, J., 1979, Kaweah serpentinite mélange, southwest Sierra Nevada foothills, California: Geological Society of America Bulletin, v. 90, p. 29-46.

Saleeby, J., 2011, Geochemical mapping of the Kings-Kaweah ophiolite belt, California – Evidence for progressive mélange formation in a large offset transform-subductioniniziation environment, *in* Wakabayashi, J., and Dilek, Y., eds., Melanges: Processes of formation and societal significance. Geological Society of America Special Paper 480, p. 31-73.

Scholl, D. W., Vallier, T.L., and Stevenson A.J., 1987, Geologic evolution and petroleum geology of the Aleutian Ridge, *in* Scholl, D. W., Grantz, A., and Vedder, J. G., eds., Geology and resource potential of the continental margin of western North America and adjacent ocean basins - Beaufort Sea to Baja California: Circum-Pacific Council for Energy and Mineral Resources, Earth Science Series, v. 6, p. 124-155, Houston, Texas.

Silver, E.A., and Beutner, E.C., 1980, Melanges: Geology: v. 8, p. 32–34.

Singlengton, J.S., and Cloos, M., 2013, Kinematic analysis of mélange fabrics in the Franciscan Complex near San Simeon, California: Evidence for sinistral slip on the Nacimiento fault zone?: Lithosphere, v. 5, p. 179-188.

Stampfi, G.M., and Borel, G.D., 2002, A plate tectonic model for the Paleozoic and Mesozoic constrained by dynamic plate boundaries and restored synthetic oceanic isochrones: Earth and Planetary Science Letters, v. 196, p. 17 - 33.

Stampfi, G.M., Borel, G.D., Marchant, R., and Mosar, J., 2002, Western Alps geological constraints on western Tethyan reconstructions, *in* Rosenbaum, G., and Lister, G.S., eds., Reconstruction of the evolution of the Alpine-Himalayan Orogen: Journal of the Virtual Explorer, v. 7, p. 75 - 104.

Strasser, M., Moore, G.F., Kimura, G., Kitamura, Y., Kopf, A.J., Lallemant, S., Park, J-O., Screaton, E.J., Su, X., Underwood, M.B., and Zhao, X., 2009, Origin and evolution of a splay fault in the Nankai accretionary check: Nature Geosciences, v. 2, p. 648–652, doi:10.1038/ngeo609.

Strasser, M., Moore, G.F., Kimura, G., Kopf, A.J., Underwood, M.B., Guo, J., and Screaton, E.J., 2011, Slumping and mass transport deposition in the Nankai fore arc: Evidence from IODP drilling and 3-D reflection seismic data: Geochemistry Geophysiscs Geosystems, v.12, Q0AD13, doi:10.1029/2010GC003431.

Taira, A., Hill, I., Firth, J., Berner, U., Bruckmann, W., Byrne, T., Chabernaud, T., Fisher, A., Foucher, J-P., Gamo, T., Gieskes, J., Hyndman, R., Karig, D., Kastner, M., Kato, Y., Lallemant, S., Lu, R., Maltman, A., Moore, G., Moran, K., Olaffson, G., Owens, W., Pickering, K., Siena, F., Taylor, E., Underwood, M., Wilkinson, C., Yamano, M., Zhang, J., 1992, Sediment deformation and hydrogeology of the Nankai trough accretionary prism: synthesis of shipboard results of ODP Leg 131: Earth and Planeteray Science Letters, v. 109, p.431–450.

Ukar, E., 2012, Tectonic significance of low-temperature blueschist blocks in the Franciscan mélange at San Simeon, California: Tectonophysics, v. 568-569, p. 154–169.

Vai, G.B., and Castellarin, A., 1993, Correlazione sinottica delle unità stratigrafiche nell'Appennino Settentrionale, *in* Capozzi, R., and Castellarin, A., eds., Studi preliminari all'acquisizione dati del profilo CROP 1-1a La Spezia-Alpi orientali: Studi Geologici Camerti, Volume Speciale 2, p. 171-185.

Vannucchi, P., and Bettelli, G., 2002, Mechanism of subduction accretion as implied from the broken formations in the Apennines, Italy: Geology, v. 30, n. 9, p. 835-838.

Vannucchi, P., and Bettelli, G., 2010, Myths and recent progress regarding the Argille Scagliose, Northern Apennines, Italy, *in* Dilek, Y., ed., Alpine Concept in Geology: International Geology Review, v. 52, nos. 10–12, p. 1106–1137.

Vannucchi, P., and Maltman, A, 2000, Insight into shallow-level processes of mountain building from the Northern Apennines, Italy: Journal of Geological Society, London, v. 157, p. 105–120.

Vannucchi, P., Maltman, A., Bettelli, G., and Clennel, B., 2003, On the nature of scaly fabric and scaly clay: Journal of Structural Geology, v, 25, p. 673-688.

Vezzani L., Festa, A., and Ghisetti, F., 2010, Geology and Tectonic evolution of the Central-Southern Apennines, Italy: Geological Society of America Special Paper 469, 58 p., accompanying by a CD-ROM including the "Geological-Structural Map of the Central-Southern Apennines (Italy)" at 1:250,000 scale, Sheets 1 and 2. doi: 10.1130/2010.2469.

Vignaroli, G.L., Faccenna, C., Jolivet, L., Piromallo, C., and Rossetti, F., 2008, Subduction polarity reversal at the junction between the Western Alps and the Northern Apennines, Italy: Tectonophysics, v. 450, p. 34-50.

von Huene, R., and Lallemand, S., 1990, Tectonic erosion along the Japan and Peru convergent margins: Geological Society of America Bulletin, v. 102, p. 704-720.

von Huene, R., Ranero, C.R., Weinrebe, W., and Hinz, K., 2000, Quaternary convergent margin tectonics of Costa Rica, segmentation of the Cocos Plate, and Central American volcanism: Tectonics, v. 19, p. 314–334, doi:10.1029/1999TC001143.

Wakabayashi, J., 2011, Mélanges of the Franciscan Complex, California: Diverse structural settings, evidence for sedimentary mixing, and their connection to subduction processes. Geological Society of America Special Papers 480, 117-141. doi: 10.1130/2011.2480(05).

Wakabayashi, J., 2012, Subducted sedimentary serpentinite mélanges: Record of multiple burial–exhumation cycles and subduction erosion: Tectonophysics. V. 568-569, p. 230-274.

Wakita, K., 2012, Mappable features of mélanges derived from Ocean Plate Stratigraphy in the Jurassic accretionary complexes of Mino and Chichibu terranes in Southwest Japan: Tectonophysics, v. 568-569, p. 74-85.

Wang, K., and Hu, Y., 2006, Accretionary prisms in subduction earthquake cycles: The theory of dynamic Coulomb wedge: Journal of Geophysical Research, v. 111, B6, p. B06410, doi: 10.1029/2005JB004094.

Yamamoto, Y., 2006, Systematic variation of shear-induced physical properties and fabrics in the Miura-Boso accretionary prism: the earliest processes during off-scraping: Earth and Planetary Science Letters, v. 244, p. 270-284.

Yamamoto, Y., Nidaira, M., Ohta, Y., and Ogawa, Y., 2009, Formation of chaotic rock units during primary accretion processes: examples from the Miura-Boso accretionary complex, central Japan: Island Arc, v. 18, p. 496-512.

Yamamoto, Y., Yamada, Y., Yamashita, Y., Chiyonobu, S., Shibata, T., Hojo, M., 2012, Systematic development of submarine slope failures at subduction margins: fossil record of accretion-related slope failure in the Miocene Hota Accretionary Complex, Central Japan, *in* Yamada, Y., Kawamura, K., Ikehara, K., Ogawa, Y., Urgeles, R., Mosher, D., Chaytor, J., and Strasser, M., eds., Submarine mass movements and their consequences. Advances in Natural and Technological Hazards Research 31, p. 355-364.

Figure captions

Figure 1 – (A) Structural sketch map of the northwestern Italy (modified from Bigi et al., 1983; Marroni et al., 2010; Mosca et al., 2010; Vezzani et al., 2010). (B) Location of Figure 1A. (C) Geological cross section across the northern sector of the *Tertiary Piedmont Basin* and Po plain (modified from Bello and Fantoni, 2002). The trace of the section is shown in Figure 1A. (D) Schematic crustal-scale cross section across the Western Alps to the *Tertiary Piedmont Basin* (modified from Roure et al., 1996; Stampfli et al., 2002). The section line is shown in Figure 1A.

Figure 2 –Paleogeographic reconstruction (in map and in section) of the western Tethyan realm in (A, B) the Late Cretaceous (modified after Stampfli and Borel, 2002 and Stampfi et al., 2002 for map view; Vignaroli et al., 2008 and Marroni et al., 2010 for section view) and (C-D) middle-late Eocene times (modified after Castellarin, 1994; Festa et al., 2010b; Mosca et al., 2010 for map view; Marroni et al., 2010, for section view).

Figure 3 – Stratigraphic columns of the External Ligurian Units in the Northern Apennines and Monferrato, and of the overlying Epiligurian and *Tertiary Piedmont Basin* successions. Modified from Marroni and Pandolfi (2007); Marroni et al. (2001, 2010); Codegone et al. (2012b).

Figure 4 – (A) Simplified geological-structural map of the study area (location in Fig. 1A), showing the structural relationships between different chaotic rock units. (B) Geological cross section.

Figure 5 – *Broken Formation*: (A) Schematic 3D drawing of an outcrop exposure (North of Gerbole) showing the different degrees of layer-parallel extension in two orthogonal directions. Asymmetrical boudinage, pinch-and-swell features, and R and R' shears characterize the WNW-striking section; symmetrical flattening and boudinage are present on the NNE-striking section. (B) Schematic 3D

1188 drawing of an outcrop exposure (North of Gerbole), showing (a) the geometry of intralayer folds that
1189 show a sheath-like geometry on the NNE-stringing section. Note the asymmetric boudinage of fold
1190 limbs on the WSW-striking section. (b) 3D model of the intralayer fold showing the curviplanar fold
1191 axis. (C) Line-drawing of a polished hand sample, showing the asymmetric boudinage associated with
1192 extensional shearing and *in situ* disruption of alternating layers of sandstone (black) and shale (white)
1193 (NW of Gerbole). Black lines indicate R-shears. (D) Photograph showing a close-up of Fig. 5C. Black
1194 lines indicate R-shears. (E) Photograph of a polished surface of hand sample showing C'-type shears
1195 (*sensu* Passchier and Trouw, 2002; see withe lines) that transecting the varicolored shaly layers
1196 (North of Piazzo). (G) SEM image showing anastomosing domains of flattened clay particles,
1197 transected by C'-type shears (*sensu* Passchier and Trouw, 2002; see white lines).
1198
1199 **Figure 6** –Diagrams showing different organizational types of the blocks and the rock fabric in diverse
1200 types of chaotic rock units: (A) Aspect ratio (blocks long axis/short axis) versus block long axis. (B)
1201 Aspect ratio (blocks long axis/short axis) versus location of chaotic units (i.e., distance from the thrust
1202 faults). Data are plotted as means with 95% error bars indicated. (C) Mesoscale data (Schmidt net,
1203 lower hemisphere) of scaly fabric, lineation of the long-axis of the blocks, and folds of *Broken*
1204 *Formation, Tectonic Mélange* and *Diapiric Mélange*.
1205
1206 **Figure 7** – *Tectonic Mélange*: (A) Line-drawing of an outcrop exposure (SW of la Pietra), showing the
1207 "structurally ordered" block-in-matrix fabric related to a NE-verging reverse shear (black lines). Dark-
1208 gray color indicates both native and exotic blocks (see text); white color indicates the shaly matrix. (B)
1209 Close-up of Fig. 7A. The photograph shows elongated to phacoidal blocks embedded in the scaly
1210 matrix that is pervasively affected by an S-C fabric. (C) Line-drawing of polished hand sample,
1211 showing the reorientation of elongated blocks (dark-gray color) to S-C fabric (black lines). White color
1212 indicates the shaly matrix (NW of Gerbole). (D) SEM image of the shaly matrix, showing the S-C fabric
1213 (white dashed lines). The arrow indicates an elongated clast aligned parallel to the C-shear surface.

Figure 8 – *Diapiric Mélange*: (A) Detailed geological map of the diapiric body located to the NE of Piazzo (location in Fig. 4A). Note the irregular rounded shape and the two-fold zonation of deformation, which is characterized by marginal and core zones (see text for major details). The intrusive contact (white dashed line) crosscuts the NW-striking bedding of the Broken formation and the structural fabric of the *Tectonic Mélange*. (B) Core zone: tabular and phacoidal limestone and sandstone blocks aligned parallel to the sub-vertical fluidal fabric of the shaly matrix (NE of Piazzo). (C) Close-up of the marginal zone: elongated calcareous marly block aligned parallel to the sub-vertical flow fabric of the varicolored shaly matrix (NE of Piazzo). (D) Close-up of the transition zone between the *Diapiric* and *Sedimentary Mélanges*: the polished surface of a hand sample in top-view showing the inclusion of part of the *Diapiric Mélange* (central part of the photograph) in a brecciated matrix, which was developed during the emplacement of the Sedimentary Mélange (NE of Pareglio). (E) SEM image of the matrix in the core zone showing irregular and convolute folds (marked by dashed white lines) affecting the clay particle alignment. Clay surfaces gently wrap around elongated and lenticular clasts (white arrows). (F) SEM image of the matrix in the marginal zone, showing the finely-spaced alignment of clay particles that define sigmoid-shaped sub-vertical domains. White arrows indicate shear surfaces.

Figure 9 – *Sedimentary Mélange* (i.e., Polygenetic argillaceous breccias)*:* (A) Highly disordered block-in-matrix fabric. Variably-shaped blocks (equidimensional, tabular, phacoidal and irregular) of limestone, sandstone, marl and siltstone randomly float in the brecciated shaly matrix (NW of Gerbole). (B) Polished surface of hand sample showing the isotropic texture of the brecciated shaly matrix of Fig. 9A. (C) Polished surface of hand sample, showing the superposition along an erosive surface (white arrows) of a brecciated lenticular body onto extensionally sheared, varicolored shaly layers (North of Piazzo). (D) SEM image of the brecciated matrix of the hand sample of Fig. 9B. Rounded and irregular-shaped clasts (dashed white lines) randomly float in a clayey matrix (dashed

1240 black lines). (F) SEM image of the brecciated matrix of the hand sample of Fig. 9C. The arrow
1241 indicates the gradual decrease of the spacing between clay particles from the clast-supported to clast-
1242 poor part of the rocks.
1243
1244 **Figure 10** – *Sedimentary Mélange* (i.e., Polygenetic argillaceous breccias)*:* (A) Simplified structural
1245 map, showing the structural relationships between different chaotic rock units and the direction of
1246 emplacement of *Sedimentary Mélange* bodies (i.e., Polygenetic argillaceous breccias). Rose diagrams
1247 show the sub-radial distribution of the direction of extensional shearing measured at the base of the
1248 Polygenetic argillaceous breccias. (B) Polished surface of hand sample of the basal part of the
1249 *Sedimentary Mélange*. Extensionally sheared layers show a planar anisotropy crosscut by low-angle
1250 extensional shear surface (R-shear) (North of Piazzo). (C) SEM image of the matrix in Fig. 10B,
1251 showing the alignment of elongated clasts and compacted clay particles truncated by C'-type shears
1252 (*sensu* Passchier and Trouw, 2002; see white arrows).
1253
1254 **Figure 11** – *Shale dike injections*: (A) Line-drawing of an outcrop exposure, showing shale dike
1255 injections (grey color) intruding into the brecciated matrix of the Polygenetic argillaceous breccias
1256 (white color). Elongated blocks (black color) are reoriented by the sub-vertical shale injections (NE of
1257 Piazzo). (B) Close-up of Fig. 11A. Dashed white lines mark the margins of the blocks and of the shale
1258 dike injections. (C) Close-up of Fig. 11A. Tabular block aligned parallel to the sub-vertical fluidal
1259 features of the shale dike injection. (D) Polished surface of hand sample showing a subvertical flame-
1260 shaped injection of red shale within the brecciated matrix of the Polygenetic argillaceous breccias.
1261 Elongated limestone and sandstone clasts are rotated and aligned parallel to the intrusive contacts
1262 (NE of Pareglio). (E) SEM image of the matrix of a shale dike injection showing irregular to isoclinal
1263 folds (white lines) affecting the flow fabric of the finely spaced clay particles. White arrows indicate
1264 rounded clasts. (F) SEM image showing a close-up of an irregular fold.
1265

Figure 12 – (A) Conceptual model for the evolution of the Ligurian accretionary wedge during the Late Cretaceous – middle Eocene (accretionary stage). Not-to-scale. (B) Block diagram showing the deformation of sediments prior to accretion. Vertical compaction of unconsolidated sediments occurs prior to accretion, forming a symmetrical boudinage. The increasing shear during the approach to the toe of the accretionary wedge promotes asymmetrical boudinage and development of R-shears in more competent layers. (C) Block diagram showing the deformation of sediments within the toe of the accretionary wedge. Heterogeneous deformation results in the contemporaneous production of flattened, intralayer, sheath like folds, layer-parallel extensional fabric, and asymmetric boudinage. This heterogeneous deformation is likely related to the inclination of sedimentary layers with respect to the $\sigma 1$ (see Kusky and Bradley, 1999). See text for a detailed discussion.

Figure 13 –Conceptual model for the evolution of the Ligurian accretionary wedge during late Oligocene intracollisional deformation. The superposition of tectonic, diapiric and sedimentary processes occurred in this short time span. (A) Thrusting related to NE-verging regional shearing formed the *Tectonic Mélange*. This is characterized by (A') a structurally ordered block-in-matrix fabric produced by mixing of the exotic and native blocks that are wrenched from the overlying units (see stratigraphic column in Fig. 13A). (B) *Diapiric Mélange* formed by the upward rise of uncosolidated sediments that are triggered by overpressurized fluids, which are concentrated along the shear surface of thrust faults. (C) *Sedimentary Mélange* (i.e., Polygenetic argillaceous breccias) formed by the collapse of the margins of the topographic high formed by the emergence of a diapiric body on the seafloor. (C') Downslope emplacement of *Sedimentary Mélanges* units sealed the thrust faults, superposing the External Ligurian Units on the late Eocene–Oligocene Tertiary Piedmont Basin sedimentary succession. Shale dike injection is triggered by the combined effect of sedimentary loading (provided by the emplacement of the *Sedimentary Mélange*) and discharge of fluids after the thrust faulting stage, intrudes into the *Sedimentary Mélange* (i.e., Polygenetic argillaceous breccias). (C'') Close-up of a shale dike injections into the block-in-matrix fabric of the *Sedimentary Mélange*.

1292

1293 **Table 1** – Diagnostic structural features observed at the map-to meso- and micro-scales in the *Broken*

1294 *Formation* and in the *Tectonic, Diapiric* and *Sedimentary Mélanges*.

Figure 1
Click here to download high resolution image

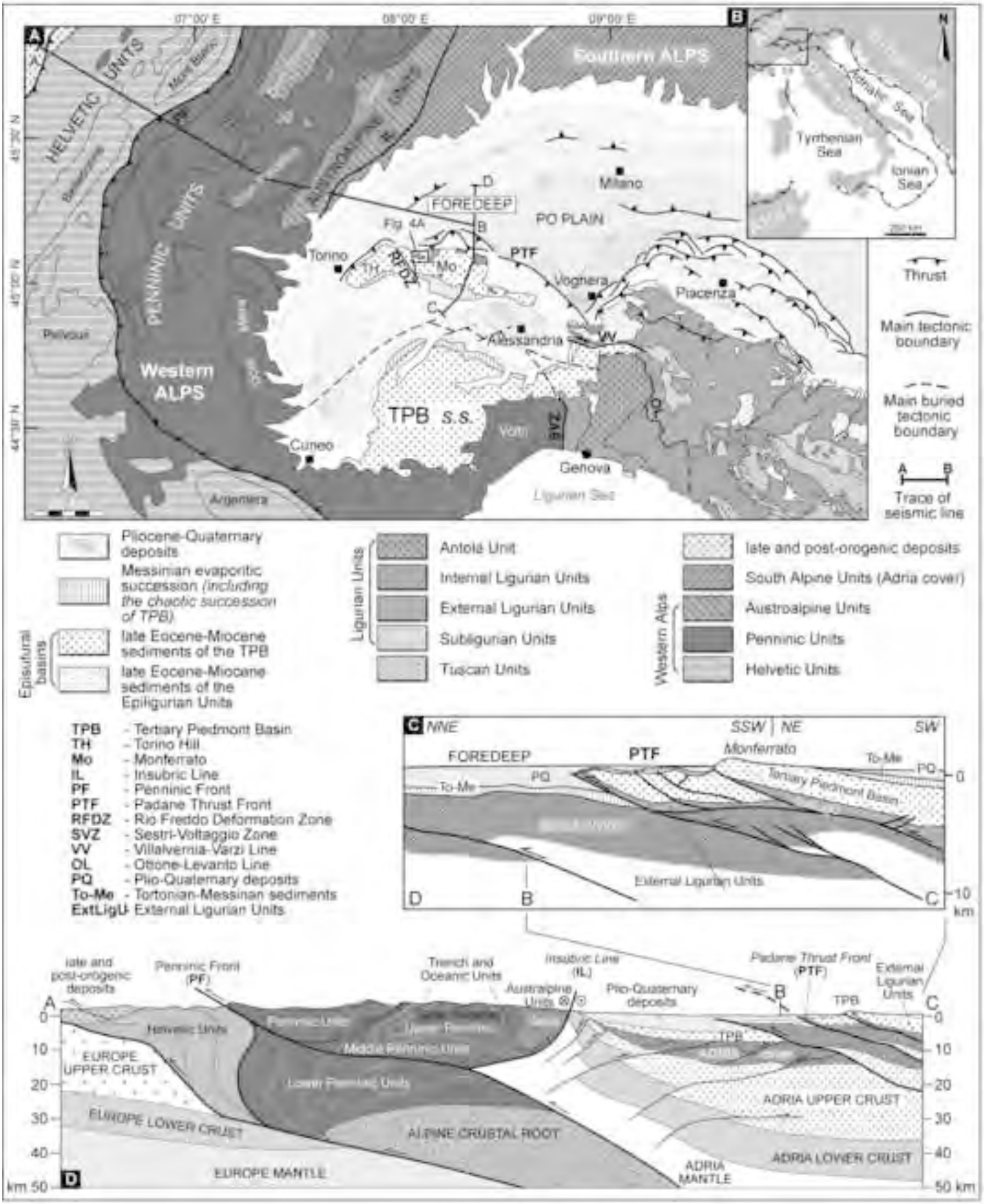

Figure 1 - Festa et al. (*.jpg)

Figure 2
Click here to download high resolution image

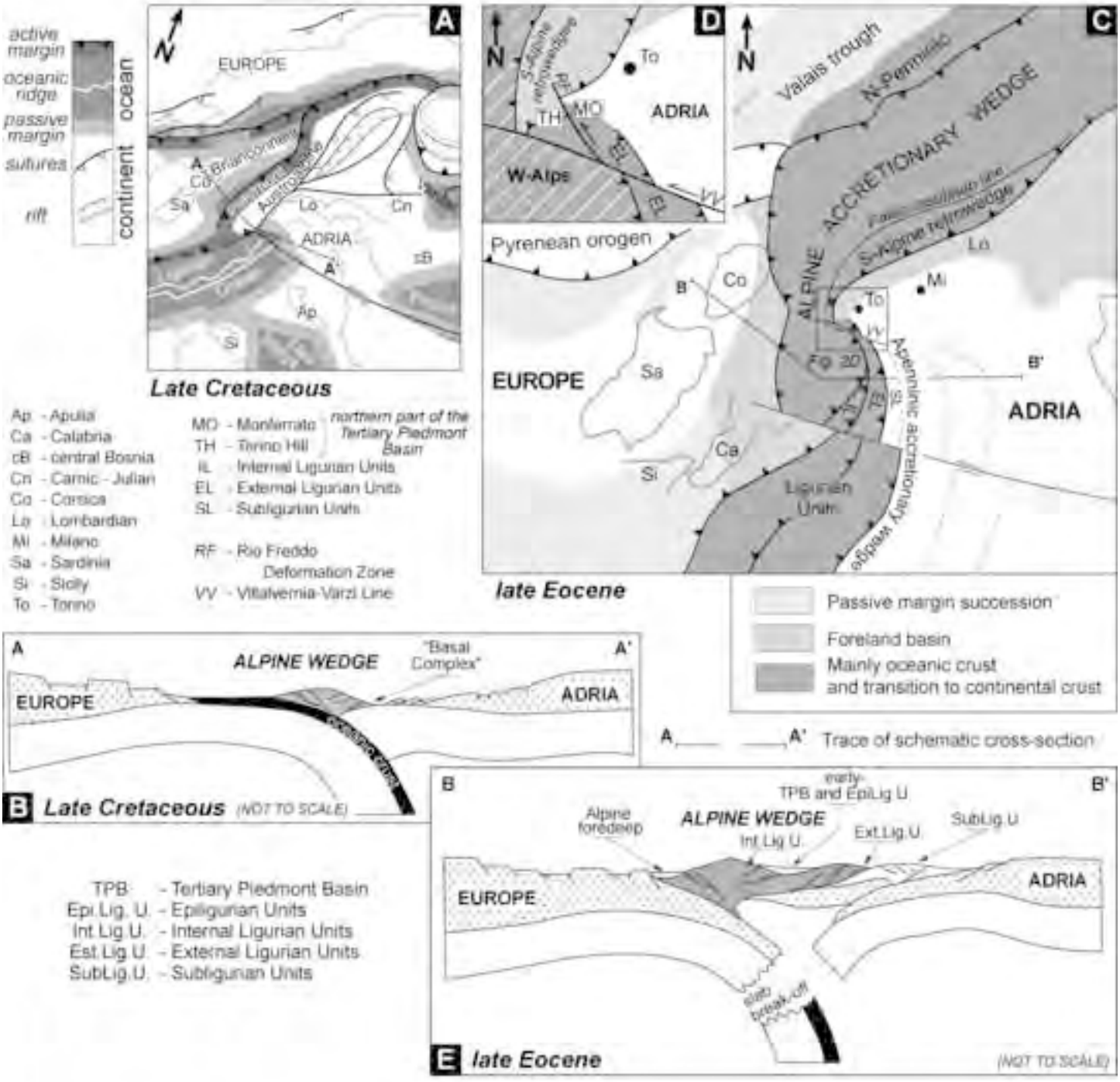

Figure 2 - Festa et al. (*.jpg)

Figure 3
Click here to download high resolution image

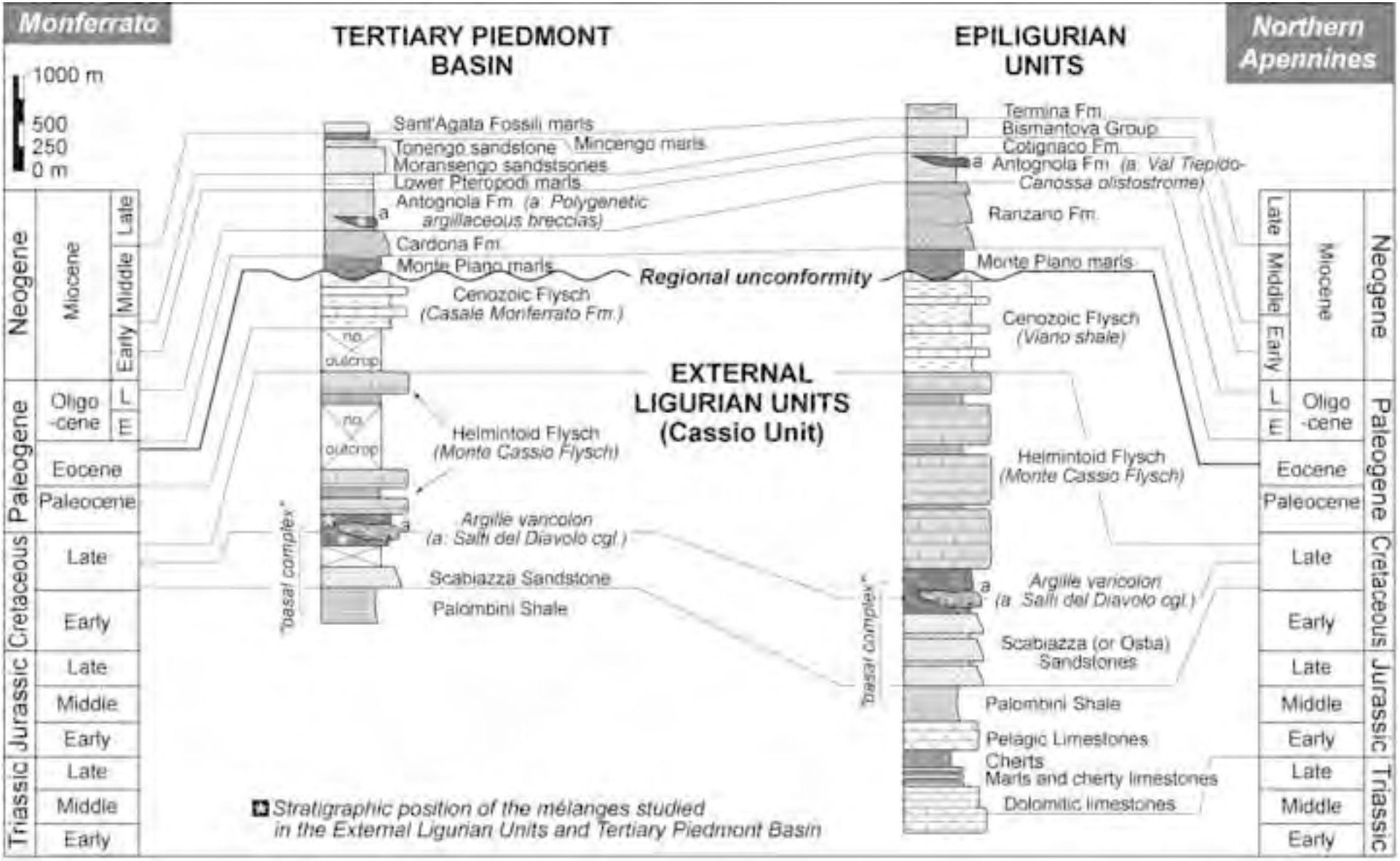

Figure 3 - Festa et al. (*.jpg)

Figure 4 (Revised)
Click here to download high resolution image

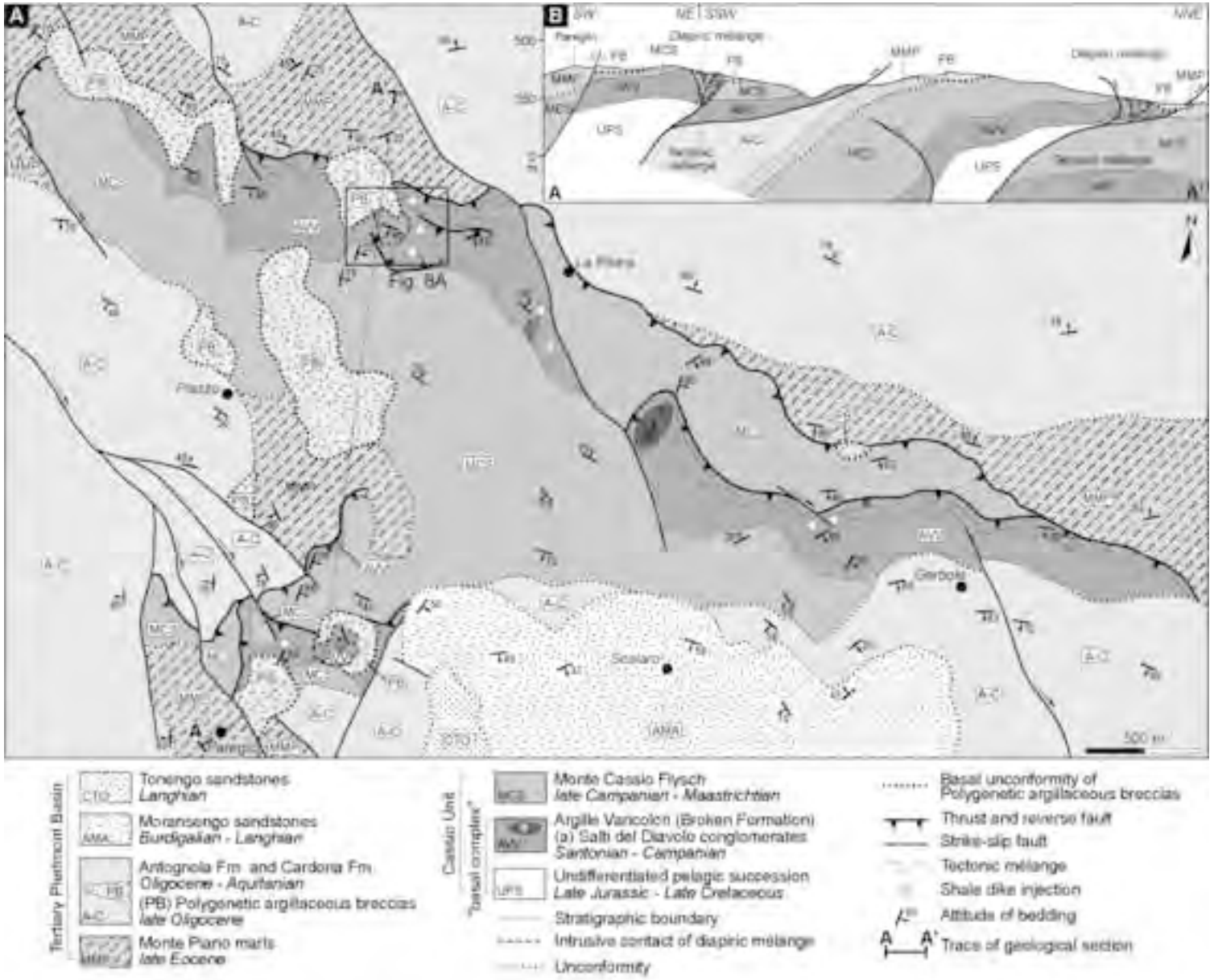

Figure 4 - Festa et al. (*.jpg)

Figure 5
Click here to download high resolution image

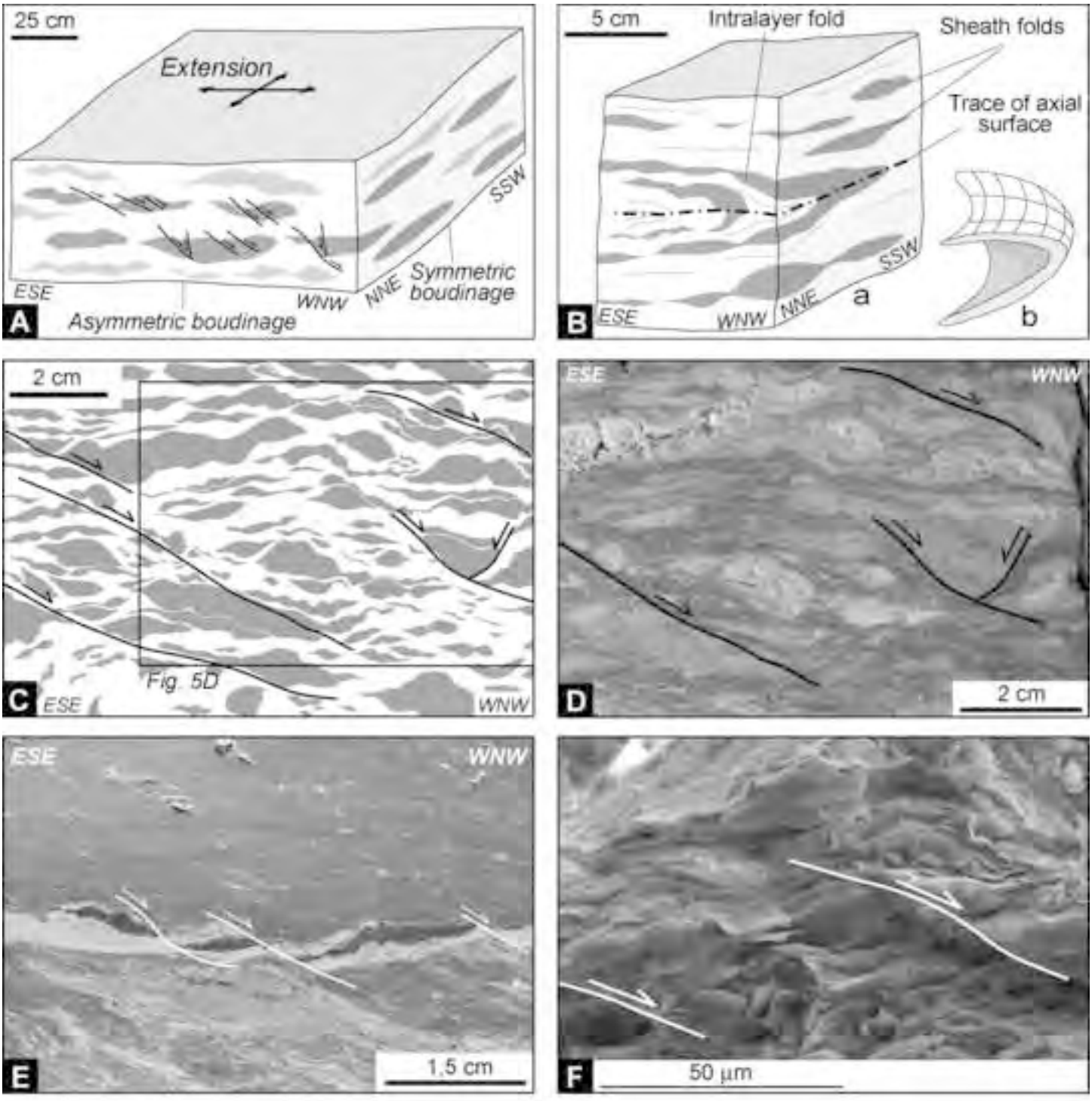

Figure 5 - Festa et al. (*.jpg)

Figure 6
Click here to download high resolution image

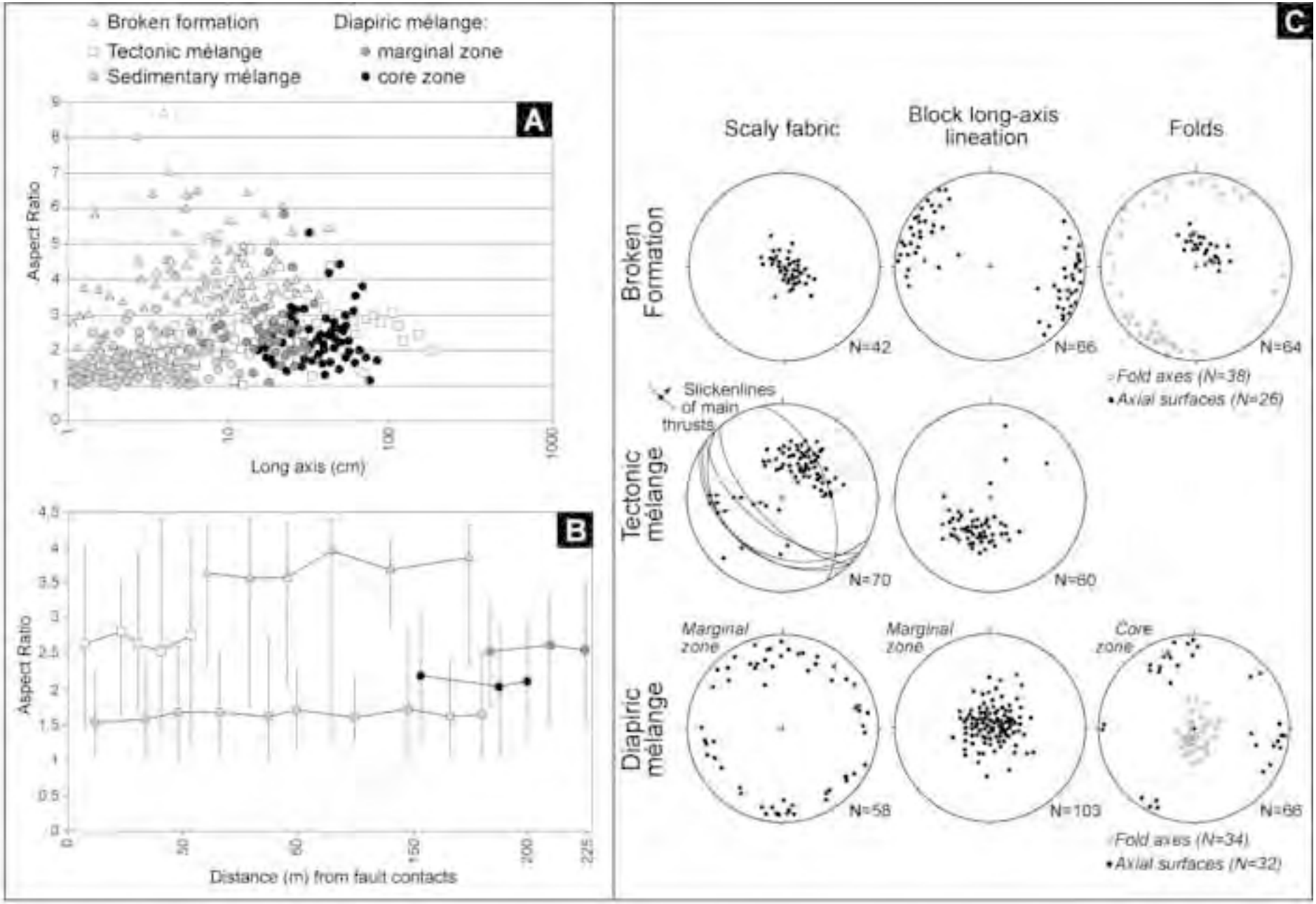

Figure 6 - Festa et al. (*.jpg)

Figure 7
Click here to download high resolution image

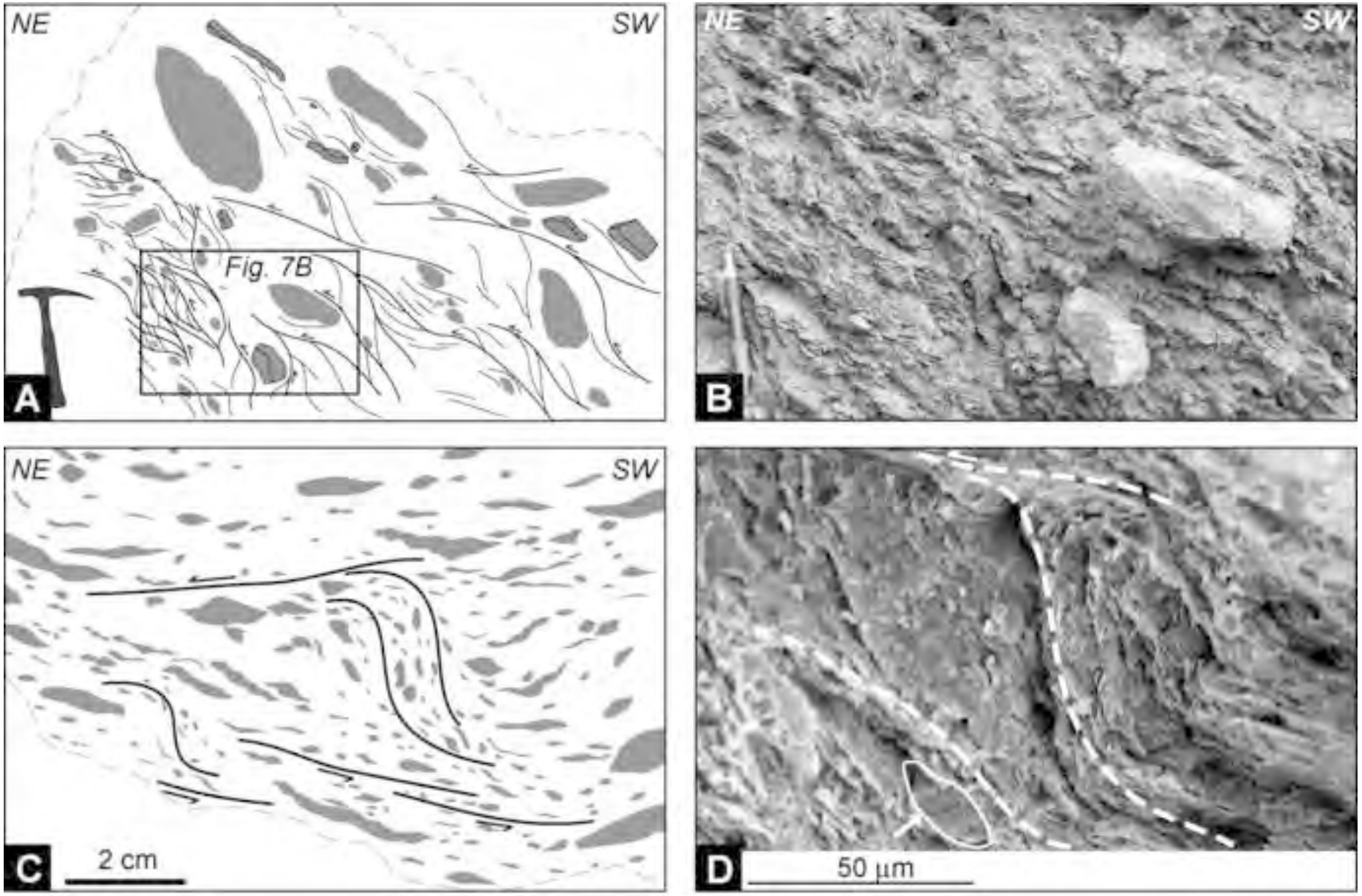

Figure 7 - Festa et al. (*.jpg)

Figure 8
Click here to download high resolution image

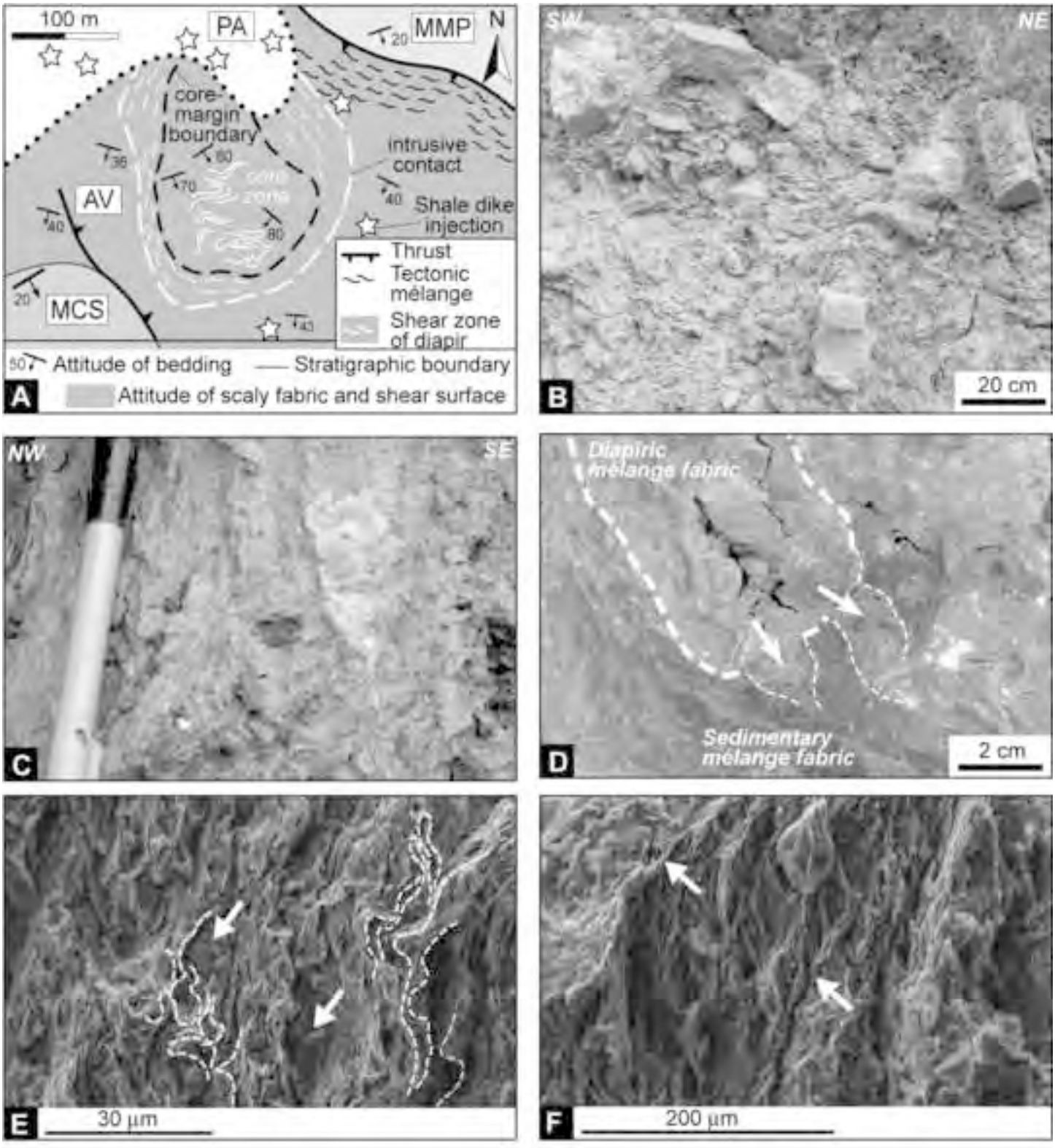

Figure 8 - Festa et al. (*.jpg)

Figure 9
Click here to download high resolution image

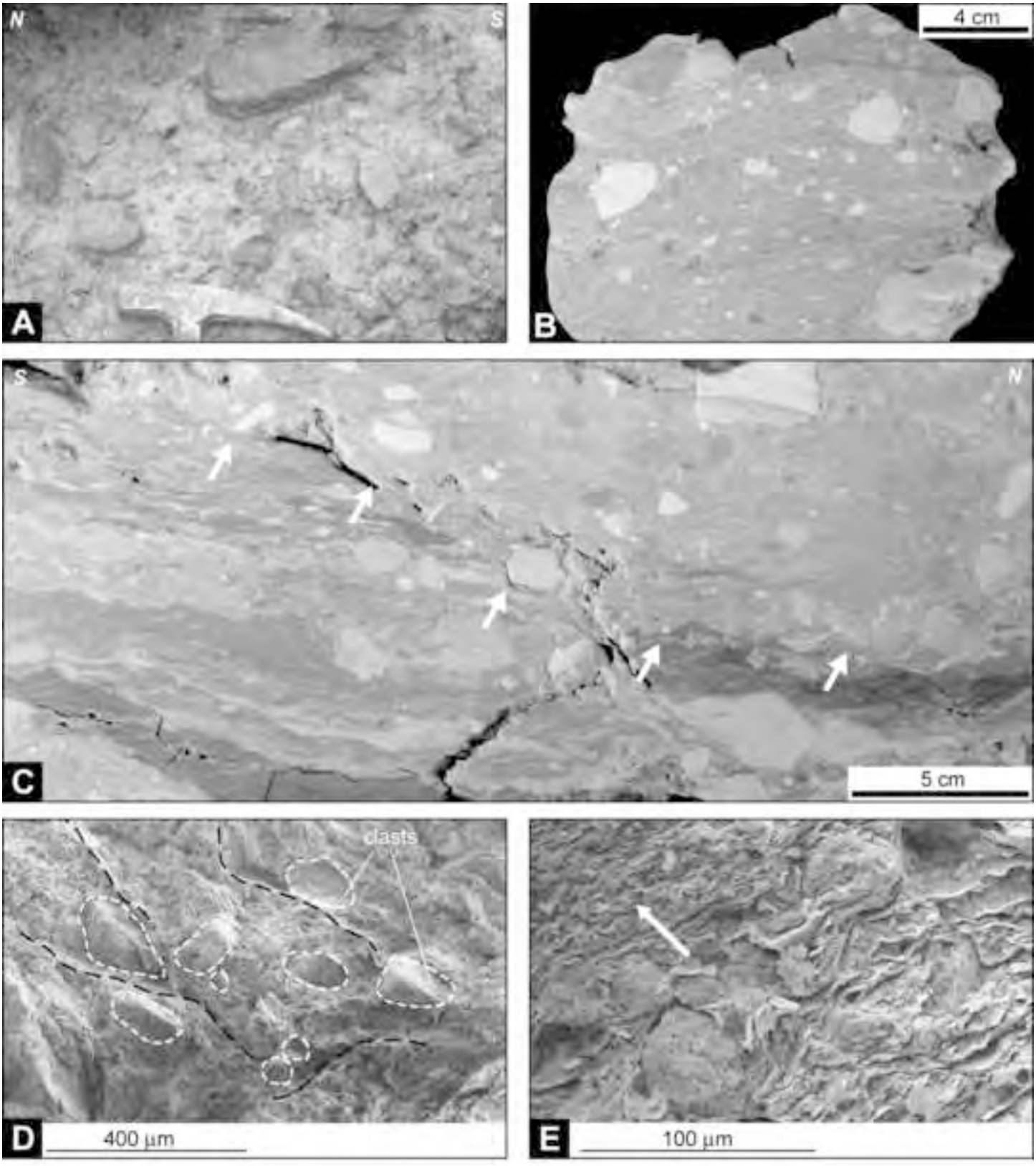

Figure 9 - Festa et al. (*.jpg)

Figure 10
Click here to download high resolution image

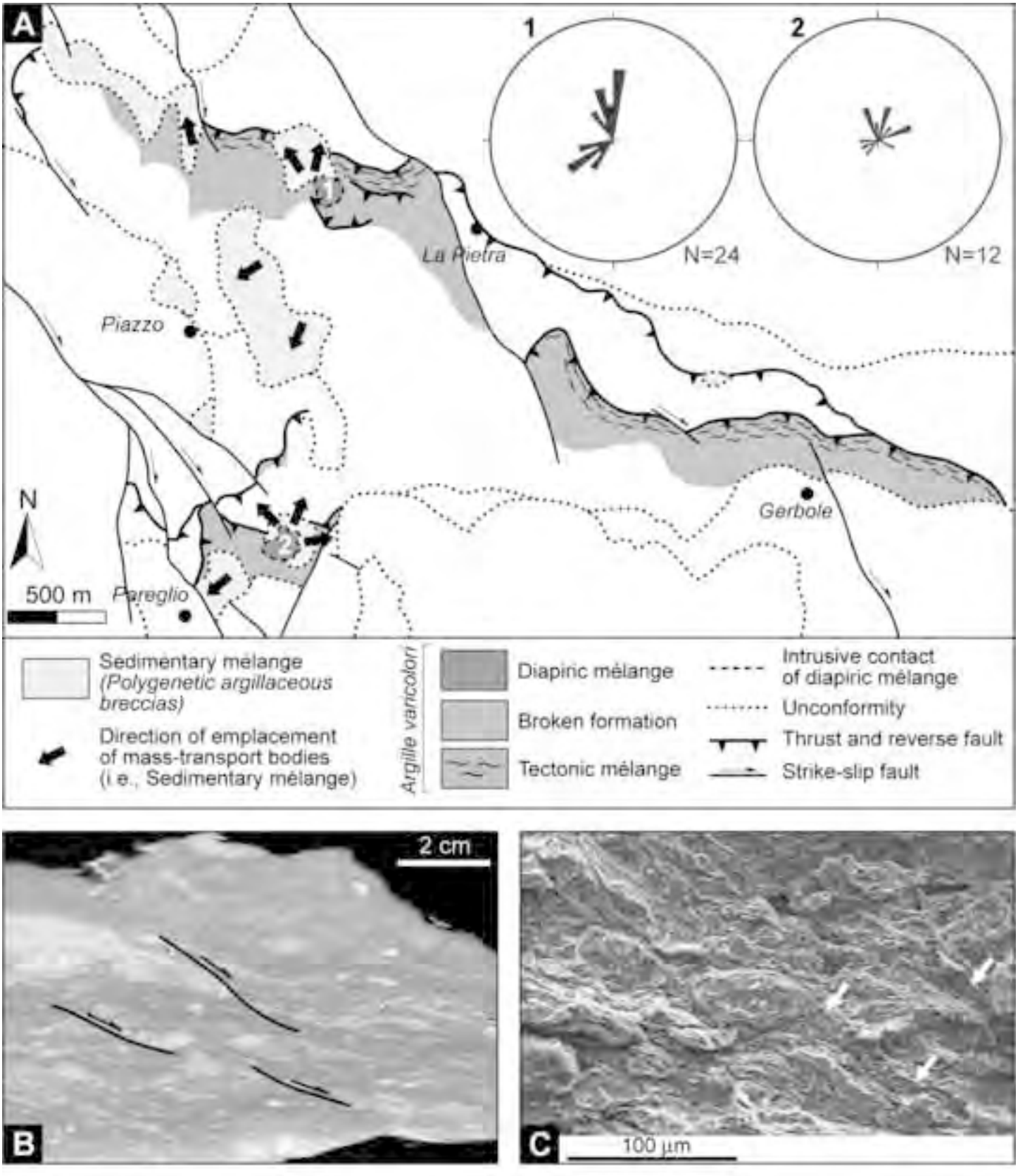

Figure 10 - Festa et al. (*.jpg)

Figure 11
Click here to download high resolution image

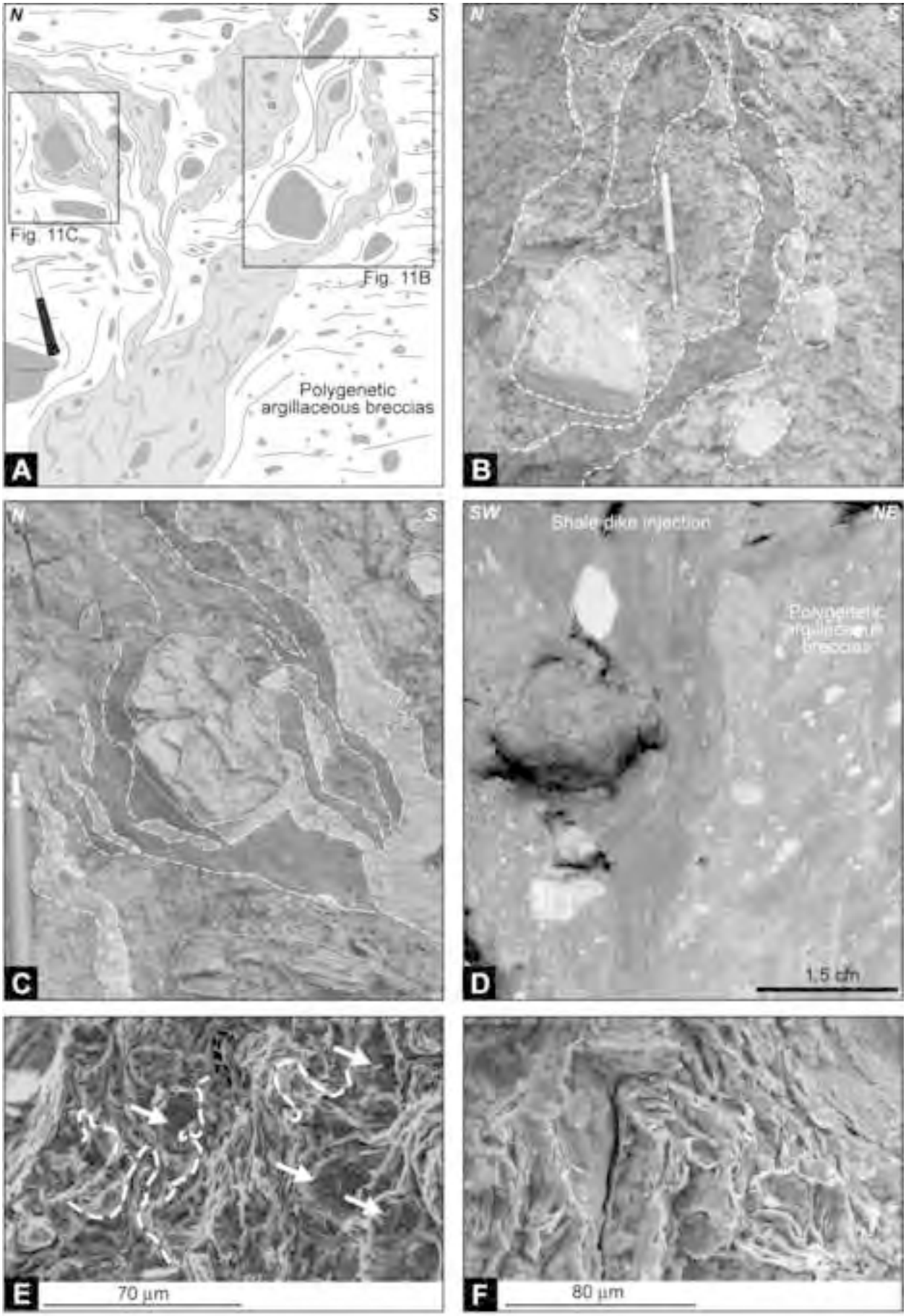

Figure 11 - Festa et al. (*.jpg)

Figure 12
Click here to download high resolution image

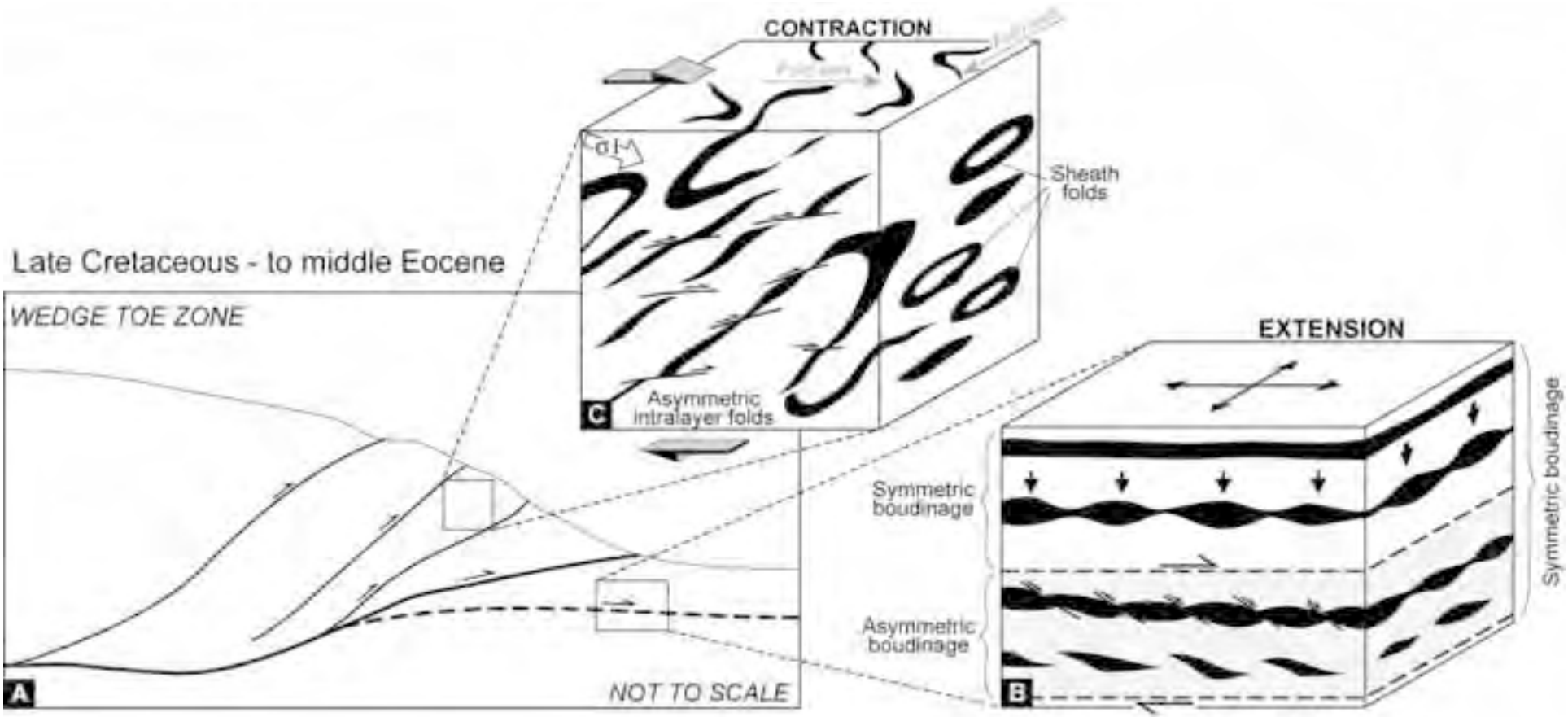

Figure 12 - Festa et al. (*.jpg)

Figure 13 (Revised)
Click here to download high resolution image

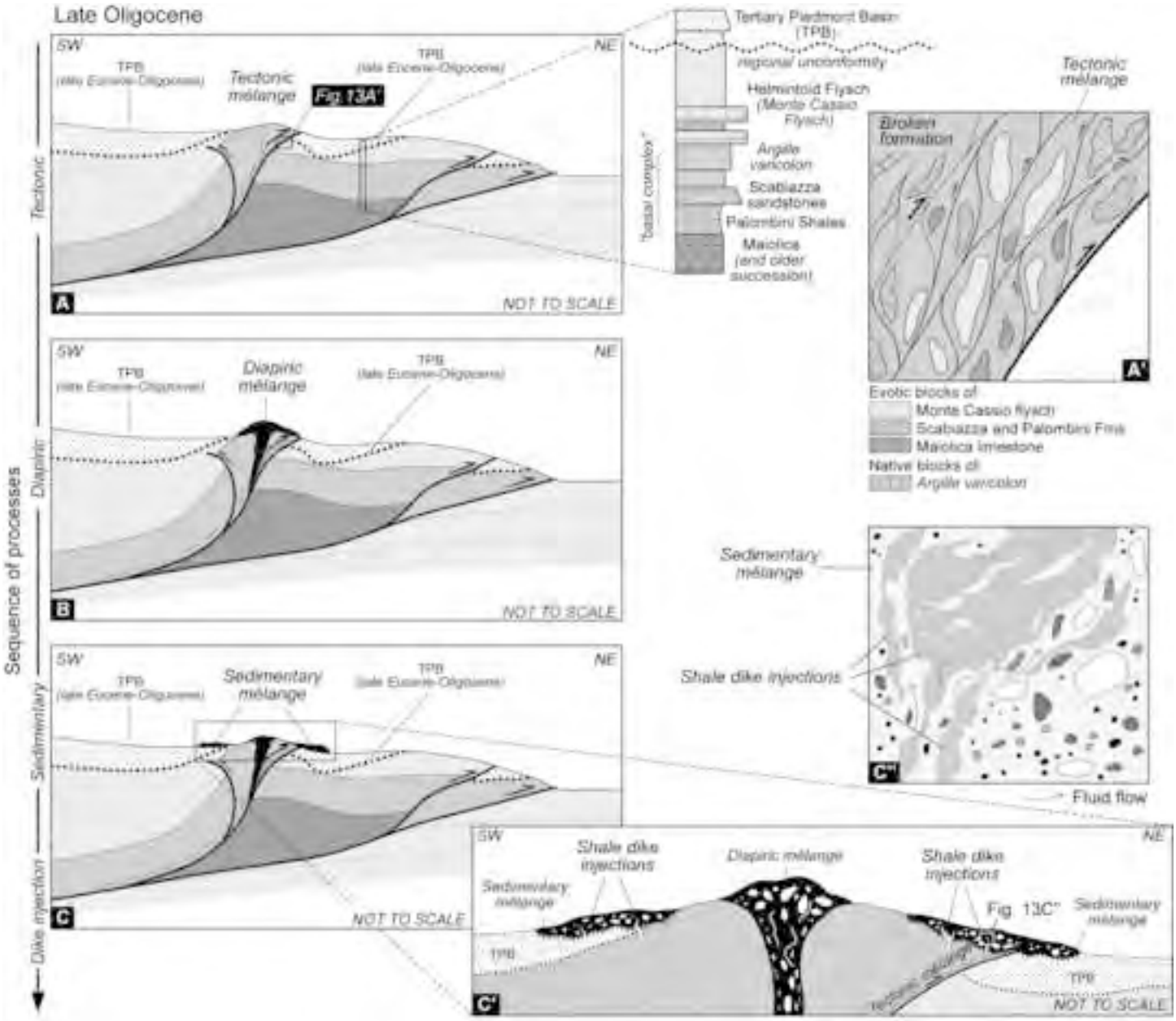

Figure 13 - Festa et al. (*.jpg)

Table 1

TABLE 1.

		Broken Formation	Tectonic Mélange	Diapiric Mélange	Sedimentary Mélange
Process of formation		Tectonic		Diapiric	Sedimentary (gravitational)
Map-scale features	**Shape of chaotic unit** (in map view)	Aligned to conformable stratigraphic contacts of bounding lithostratigraphic units	Narrow and elongated; aligned to thrusts	Circular to elliptical	Irregular
	Nature of bounding surface	No bounding surface: gradual transition to both Tectonic Mélange and coherent lithostratigraphic units	Fault (i.e., thrust)	High angle intrusive contacts	Lower and upper depositional contacts as discontinuity surfaces
Meso-scale features	**Block-in-matrix fabric**	Progressive distribution from continuous layering to boudinage up to isolated blocks aligned to the original coherent bending (i.e., pseudo-bedding) Non-cylindrical, flattened intralayer folds wi h curviplanar axial surfaces	Structurally ordered fabric (S-C and/or P-T shears) consistent with the regional shortening direction	Zonation of deforma ion: - Core zone: plurimetric, irregular non-cylindrical folds with steeply dipping axes and irregular axial trends; - Marginal zone: pervasive vertical scaly fabric and fluidal features which wrap around the blocks	Random distribution of blocks in a brecciated isotropic matrix
	Nature of blocks	Native (i.e., intra-formational)	Native (i.e., intra-formational) and exotic (i.e., extra-formational)		
	Shape of blocks	From flat to ellipsoidal shape (aspect ratio: 3,5-4)	Phacoidal and tabular blocks (aspect ratio: 2,5-2,8)	- Core zone: irregular blocks (aspect ratio: 2,1-2,3) - Marginal zone: phacoidal blocks (aspect ratio: 2,5-2,6)	Angular to rounded and irregular blocs (aspect ra io: 1,5-1,7)
	Size of blocks	mean: 33 cm max: 50 cm	- Native blocks: mean: 33 cm; max: 50 cm - Exotic blocks: mean: 35 cm; max: 125 cm	- Core zone: mean: 60 cm; max: 90 cm - Marginal zone: mean: 25 cm; max: 40 cm Sub-vertical flow fabric.	mean: 4 cm max: 15 cm
Micro-scale features	**Matrix fabric**	Anastomosing domains of clays aligned to bedding. Locally, the fabric is transected by C' and/or R shears	Clays rotated and aligned to S-C fabric which isolate sigmoidal to lenticular shaped micro-lithons. Occurrence of striation.	- Core zone: alignment of irregularly anastomosing and folded clays (sub-vertical axial fold); - - Marginal zone: sub-vertical S-C fabric	Anastomosing domains of clays that, close to the basal erosional surface, are transected by C'-type shears
	Clast arrangement	Planar orientation of elongated clasts, locally transected by R-shears	Alignment of elongated clasts to he S-C fabric	Alignment of elongated clasts to the fluidal fabric	Random distribution of equidimensional and irregular clasts. Close to the basal surface, elongated clasts are aligned to the clays

Table 1 – Festa et al. (*.doc)